PHOTONICS Research

Review on metal halide perovskite-based optoelectronic synapses

Xitong Hong,[1] Xingqiang Liu,[2,3] Lei Liao,[2,4] and Xuming Zou[1,2,5]

[1]Key Laboratory for Micro/Nano Optoelectronic Devices of Ministry of Education & Hunan Provincial Key Laboratory of Low-Dimensional Structural Physics and Devices, School of Physics and Electronics, Hunan University, Changsha 410082, China
[2]State Key Laboratory for Chemo/Biosensing and Chemometrics, College of Semiconductors (College of Integrated Circuits), Hunan University, Changsha 410082, China
[3]e-mail: liuxq@hnu.edu.cn
[4]e-mail: liaolei@whu.edu.cn
[5]e-mail: zouxuming@hnu.edu.cn

Received 16 November 2022; revised 2 February 2023; accepted 4 February 2023; posted 6 February 2023 (Doc. ID 480057); published 28 April 2023

With the progress of both photonics and electronics, optoelectronic synapses are considered potential candidates to challenge the von Neumann bottleneck and the field of visual bionics in the era of big data. They are also regarded as the basis for integrated artificial neural networks (ANNs) owing to their flexible optoelectronic tunable properties such as high bandwidth, low power consumption, and high-density integration. Over the recent years, following the emergence of metal halide perovskite (MHP) materials possessing fascinating optoelectronic properties, novel MHP-based optoelectronic synaptic devices have been exploited for numerous applications ranging from artificial vision systems (AVSs) to neuromorphic computing. Herein, we briefly review the application prospects and current status of MHP-based optoelectronic synapses, discuss the basic synaptic behaviors capable of being implemented, and assess their feasibility to mimic biological synapses. Then, we focus on the two-terminal optoelectronic synaptic memristors and three-terminal transistor synaptic phototransistors (SPTs), the two essential apparatus structures for optoelectronic synapses, expounding their basic features and operating mechanisms. Finally, we summarize the recent applications of optoelectronic synapses in neuromorphic systems, including neuromorphic computing, high-order learning behaviors, and neuromorphic vision systems, outlining their potential opportunities and future development directions as neuromorphic devices in the field of artificial intelligence (AI). © 2023 Chinese Laser Press

https://doi.org/10.1364/PRJ.480057

1. INTRODUCTION

The sustainable development of conventional computers with von Neumann architecture and silicon complementary metal–oxide semiconductor (CMOS)-based hardware has been hampered as follows: (i) devices restricted by scaling theory near the limits of physics; (ii) von Neumann bottleneck due to physically separated storage and data processing units [1–4]. As the highest structure of the nervous system, the human brain is responsible for processing information received by various senses, an activity that depends on the existence of 100 billion neurons and 1000 trillion synapses interconnected in the cerebral cortex at an ultra-high density [5–7]. In contrast, the human brain can execute complex tasks such as parallel computation and cognitive learning with the advantages of being highly fault-tolerant and event-driven, thus generating interest in brain-like computers [8–10]. Over the past few years, significant progress has been achieved regarding brain-like chips, among which the best-known one is the TrueNorth chip introduced by IBM in 2014 [11–13]. However, since such chips for high-speed computation still suffer from low integration density and high energy consumption compared with the human brain due to the limitations of the traditional CMOS structure, the emergence of synaptic electronics will lead to the future of artificial intelligence (AI).

Inspired by biological synapses, several emerging devices with the advantages of simple device structure and high-density integration, such as phase-change memories, resistive switching memories, and field effect transistors, were proposed to mimic the synaptic plasticity [14–19]. To date, our comprehension concerning the complex characteristics of synaptic devices remains at a preliminary level, with a growing appreciation of the essential role played by both material selection and signal modulation. Despite enormous efforts that have been devoted to investigating electrical synapses, the all-electronic design raises issues of high energy consumption, limiting further applications in artificial neural networks (ANNs) [20]. Here,

taking into account the important role played by artificial vision systems (AVSs) in neuromorphic engineering, optoelectronic synapses exhibiting excellent characteristics in terms of large bandwidth and low power consumption have been developed as the foundation for the next generation of neuromorphic systems [21,22]. So far, metal oxide films, organic semiconductors, and other materials have been successively employed in synaptic devices modulated by light signals or photoelectric synergistic properties [23–28].

Metal halide perovskites (MHPs) have emerged as revolutionary photosensitive materials with the generic formula ABX3, in which A represents the cation, B denotes the divalent metal ion, and X refers to the halide [29–31]. In the past few years, the family of MHP materials has drawn considerable attention for being employed in a wide range of electronic devices like solar cells, light-emitting diodes, photodetectors, phototransistors, memory devices, flexible devices, and lasers, attributed to their superior combination of optoelectronic properties, including large light absorption coefficients, long carrier lifetimes/diffusion lengths, decent charge carrier mobility, and low exciton binding energies [32–45]. Interestingly, compared to conventional organic and inorganic materials, electronic devices employing MHPs tend to exhibit ubiquitous hysteresis effects, a phenomenon that motivates MHPs materials to serve as the most desirable contenders for simulating biological synapses, typically attributed to the inherent ion migration properties or charge carrier traps of MHPs [46–50]. To date, multiple types of optoelectronic synaptic devices based on MHPs have been developed, leveraging the dependence in synaptic plasticity upon optical pulses, and they hold the promise of constructing multifunctional artificial neuromorphic systems that perceive external environmental changes as well as the processing of performance information, in addition to accomplishing brain-like computational behaviors for higher-order learning and handwritten digit recognition [51–53].

In this manuscript, the current status and applications of MHP-based optoelectronic synapses during recent years are comprehensively summarized in Fig. 1 [23,54–60]. A brief description of the synaptic functions of the optoelectronic synaptic devices is presented in Section 2, as well as the calculation regarding the energy consumption involved in the synaptic events. Focusing on device architecture, Section 3 discusses in detail MHP-based optoelectronic synapses from the perspectives of both structural design and potential physical mechanisms, providing innovative approaches for the exploitation of the novel artificial synapses. Subsequently, the innovative functional neuromorphic applications utilizing MHP-based synaptic devices for associative learning, emotional learning, logical functions, arithmetic operations, and neuromorphic visual systems (NVSs) are further reviewed in Section 4. In conclusion, the obstacles and challenges surrounding the optoelectronic synapse are outlined in Section 5, along with reasonable predictions related to their applications.

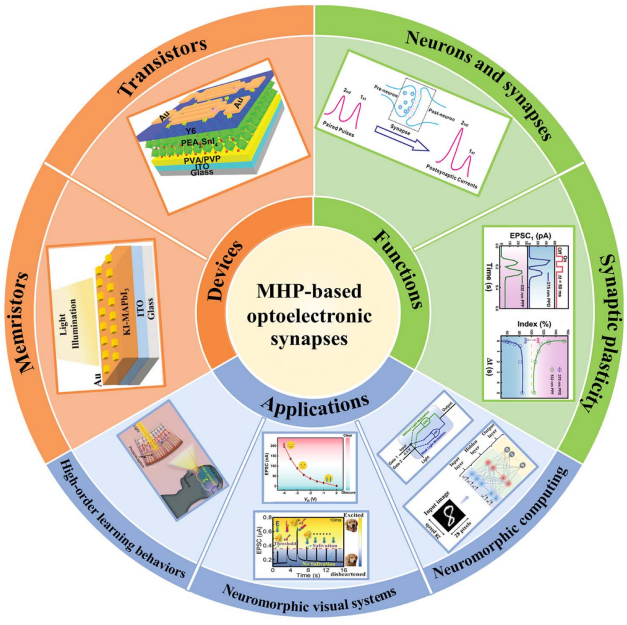

Fig. 1. Overview of this review. Neurons and synapses reprinted with permission from [54]. Copyright 2013, American Institute of Physics. Synaptic plasticity reprinted with permission from [55]. Copyright 2022, Wiley-VCH. Neuromorphic computing reprinted with permission from [56], copyright 2022, Elsevier, and from [57], copyright 2022, Wiley-VCH. Neuromorphic visual systems reprinted with permission from [23], copyright 2020, American Chemical Society, and from [58], copyright 2020, Wiley-VCH. High-order learning behaviors reprinted with permission from [59]. Copyright 2020, Wiley-VCH. Memristors reprinted with permission from [23]. Copyright 2020, American Chemical Society. Transistors reprinted with permission from [60]. Copyright 2021, Wiley-VCH.

2. BIOLOGICAL SYNAPSES AND BASIC SYNAPTIC BEHAVIOR

Synapses, as an essential component of information transmission throughout the nervous system, provide a suitable imitation object for researchers to build ANNs. In recent years, more and more MHP-based optoelectronic synaptic devices have been proposed to mimic the basic functions of biological synapses, such as synaptic plasticity [51,57,61,62]. In Section 2, the connection between neurons and synapses is described, followed by a highlight of the typical synaptic behavior of MHP-based optoelectronic synaptic devices and their performance metrics. How to achieve these synaptic behaviors with as little energy consumption as possible remains a great challenge for the construction of the devices [63–66].

A. Neurons and Synapses

Neurons, also called nerve cells, are the most basic structural and functional units of the biological nervous system. Synapses are located between two neurons that are in contact with each other and assume the function of transmitting information in a unidirectional manner within the nervous system. There are two types of biological synapses: chemical synapses and electrical synapses, which use chemical and electrical signals to transmit information, respectively. In this work, we focus on the working mechanism of chemical synapses. As shown in Fig. 2(a), a synapse consists of a combination of a presynaptic membrane, a postsynaptic membrane, and a narrow space between them (the synaptic cleft).

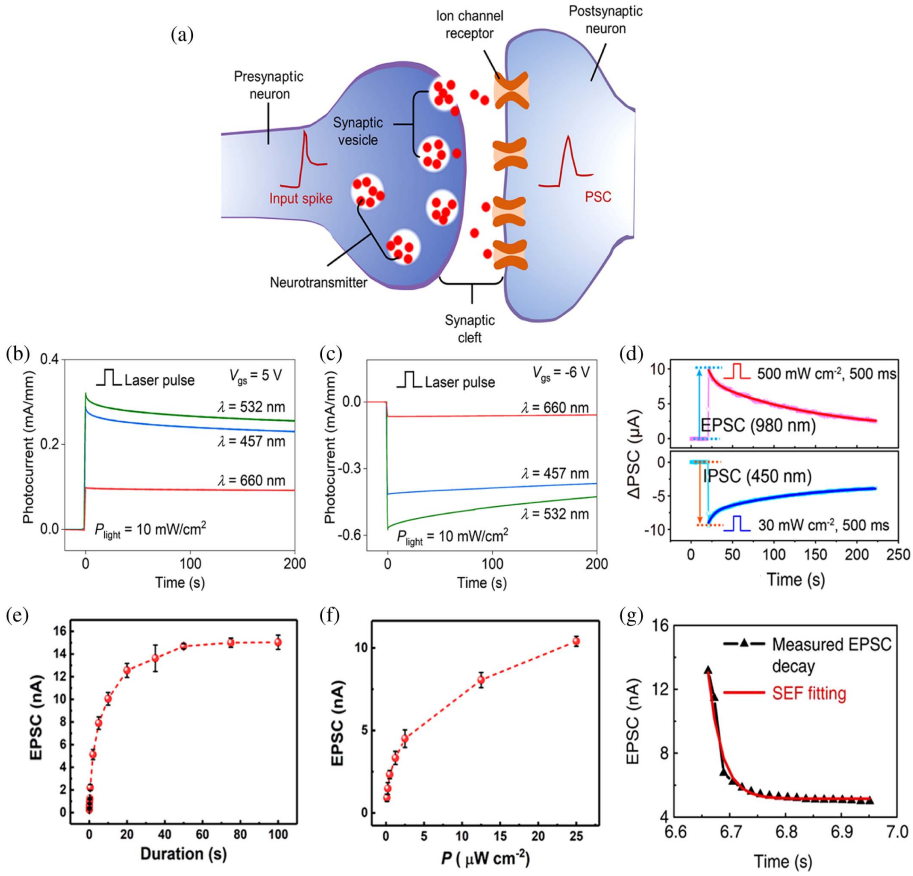

Fig. 2. (a) Structural schematic diagram of the biological synapse. (b) and (c) EPSC/IPSC of the perovskite-gated synaptic device triggered by an optical stimulus when the gate voltage is 5 V/−6 V. Reprinted with permission from [67]. Copyright 2022, John Wiley and Sons. (d) EPSC/IPSC triggered by a 980 nm/450 nm optical pulse for synaptic transistor based on the Pyr-GDY/Gr/PbS-QD heterojunction. Reprinted with permission from [68]. Copyright 2001, Elsevier. (e) and (f) EPSC as a function of pulse duration/power density for synaptic transistors based on the $MAPbI_3$/SiNM heterojunction. Reprinted with permission from [23]. Copyright 2020, American Chemical Society. (g) Typical decay of the PSC as a function of time. Reprinted with permission from [69]. Copyright 2014, Nature Portfolio.

When a nerve impulse is transmitted to the presynaptic membrane, voltage-gated calcium ion channels in the membrane open, and extracellular Ca^{2+} enters the presynaptic element, allowing neurotransmitters to be released into the synaptic cleft [70]. Some neurotransmitters bind to the corresponding receptors on the postsynaptic membrane, resulting in the opening of chemically gated channels through which the corresponding ions enter the postsynaptic element [71]. If excitatory neurotransmitters are released from the presynaptic membrane, which increases the permeability of the postsynaptic membrane to Na^+ and K^+ increases, resulting in a localized depolarization potential—that is, an excitatory postsynaptic potential (EPSP)—then the synapse is referred to as an excitatory synapse. Conversely, if the presynaptic membrane releases inhibitory neurotransmitters that increase the permeability of the postsynaptic membrane to Cl^-, leading to a local hyperpolarization potential, or inhibitory postsynaptic potential (IPSP), then the synapse is called an inhibitory synapse. It is worth noting that there are many synapses in a neuron. When the sum of the excitatory synaptic activity in the neuron exceeds the sum of the inhibitory synaptic activity and action potentials in the axons of the neuron are triggered, leading to the occurrence of nerve impulses, the neuron is presented as excitatory and, conversely, as inhibitory.

B. Synaptic Plasticity

During this dynamic process of neurons transmitting information, the strength of the connection between them is determined by the synaptic weight [68,72]. For biological nervous systems, variations in synaptic weights are defined as synaptic plasticity, which causes postsynaptic currents (PSCs) to fluctuate in response to the activity of presynaptic neurons and is regarded as fundamental to the human brain's ability to recognize, encode, store memories, and discriminate information [73,74].

1. EPSC/IPSC

For synaptic devices, external stimuli such as optical/electrical pulses applied to the electrodes correspond to the release of nerve impulses in biological synapses. The channel conductance is equivalent to the synaptic weight, and the resulting channel currents are referred to as excitatory postsynaptic current (EPSC) or inhibitory postsynaptic current (IPSC), corresponding to EPSP and IPSP of biological synapses, respectively. In general, the value of the PSC is determined by the synaptic

weights. As the most fundamental synaptic behavior that can be observed in optoelectronic synaptic devices, PSC is regarded as an essential component of ANNs. As shown in Figs. 2(b) and 2(c), PSC occurs when the perovskite-gated synaptic device is stimulated by a single light pulse. Here, EPSC or IPSC is controlled by the gate voltage of the synaptic device [67]. In addition to the modulation of the gate voltage, the wavelength of the optical stimulus is also significant in affecting the PSC [60,75]. Hou *et al.* reported an ambipolar optoelectronic synaptic device based on a Pyr-GDY/graphene/PbS quantum dot (Pyr-GDY/Gr/PbS-QD) heterojunction. As shown in Fig. 2(d), the triggered IPSC is converted to EPSC when the wavelength of the incident optical pulse is switched from 450 to 980 nm [75]. Furthermore, for synaptic devices, the magnitude of the PSC is determined by the strength and duration of the applied light/electrical pulse, as shown in Figs. 2(e) and 2(f) [23]. The decay of PSC with time after the pulse applied to the device has disappeared can be perfectly fitted by the Kohlrausch stretched exponential function (SEF) [76–80],

$$I = (I_0 - I_\infty)\exp\left[-\left(\frac{t - t_0}{\tau}\right)^{\beta}\right] + I_\infty, \tag{1}$$

where I_0 and t_0 stand for the PSC and time when the pulse stimulation ceased, respectively; I_∞ denotes the value at the final stabilization of the current; and τ and β refer to the retention time and the stretch index in the range 0–1, respectively. Figure 2(g) shows a typical decay curve of EPSC with time [69], from which it can be seen that the value of EPSC decreased first and then tended to be stable, closely matching the curve fitted according to the SEF.

2. PPF/PPD

A pair of pulse stimuli is applied to the synapse, as shown in Fig. 3(a), which modifies the concentration of Na^+/Mg^+ and other ions that contribute to the change in the postsynaptic membrane potential, which in turn affects the magnitude of the PSC after the two stimulations [54], causing a variation in the degree of connectivity between the two adjacent neurons [72]. Similarly, if two consecutive pulses of stimulation are applied to the synaptic device, the spikes of PSCs obtained from the first and second stimuli are denoted as A_1 and A_2, respectively. If the value of A_2 is larger than A_1, which implies an enhanced postsynaptic response, then this synaptic behavior is described as paired-pulse facilitation (PPF); conversely, the phenomenon indicates a depressed postsynaptic response, as well defined as paired-pulse depression (PPD) [83]. The dependence of PPF/PPD behavior on the pulse interval time makes it assume an important role in decoding the temporal data in the synaptic signal [84,85]. Wang *et al.* proposed a synaptic device based on MoS_2/PTCDA heterostructure and obtained typical PPF/PPD behavior by applying a pair of gate pulse stimuli to it [Figs. 3(b) and 3(c)] [81]. The PPF/PPD index can be calculated based on the classical equation $(A_2/A_1) \times 100\%$ or $[(A_2 - A_1)/A_1] \times 100\%$ to calculate [54,55]. Interestingly, the facilitation/depression percentage gradually decays/strengthens to 100% with the increase of

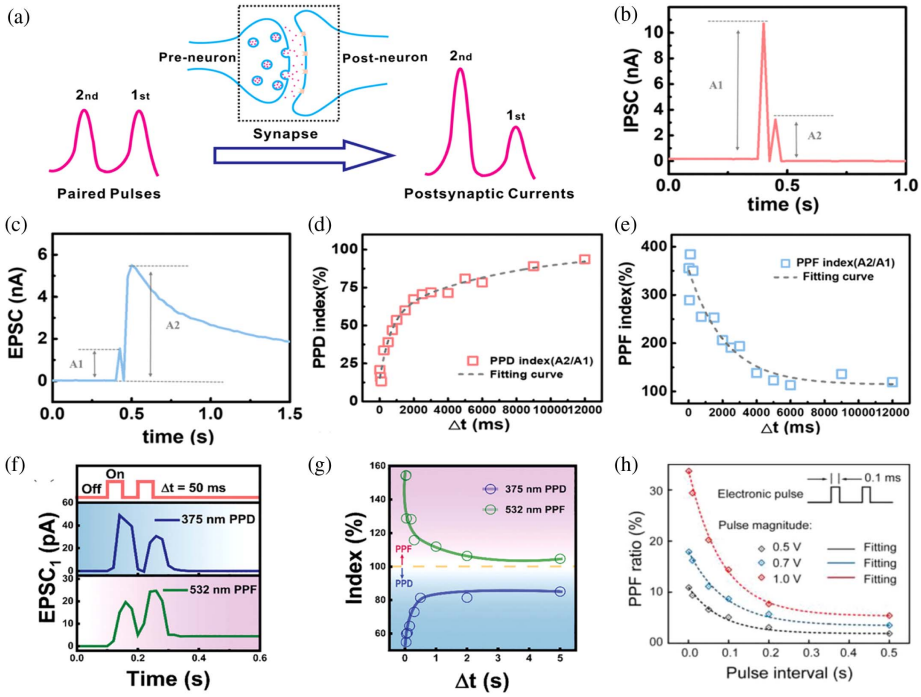

Fig. 3. (a) Schematic diagram of typical PPF/PPD behavior of synapses with two successive pulse stimuli. Reprinted with permission from [54]. Copyright 2013, American Institute of Physics. (b) and (c) IPSC/EPSC curves of heterojunction synaptic devices stimulated by two consecutive pulses. (d) and (e) The PPD/PPF index obtained as a function of stimulus pulses applied with different Δt, where the dashed line represents the fitted curve based on Eq. (2). (b)–(e) Reprinted with permission from [81]. Copyright 2019, Wiley-VCH. (f) PPF/PPD effect triggered by a pair of 532 nm/375 nm optical pulses. (g) PPF/PPD index as a function of Δt stimulated by 532 nm/375 nm optical pulses. (f) and (g) Reprinted with permission from [55]. Copyright 2022, Wiley-VCH. (h) PPF ratio as a function of pulse interval stimulated with different electrical pulse peaks. Reprinted with permission from [82]. Copyright 2019, Wiley-VCH.

pulse interval time, and the attenuation/enhancement curve can be well fitted by the following double-exponential function [Figs. 3(d) and 3(e)] [21,54,68,74,75,84]:

$$\mathrm{PPFindex} = 1 + C_1 \exp(-\Delta t/\tau_1) + C_2 \exp(-\Delta t/\tau_2), \quad \textbf{(2)}$$

where C_1 and C_2 are defined as the initial facilitation constants of the biological synapse; τ_1 and τ_2 are considered as fast and slow characteristic relaxation times, respectively, which can be extracted from the fitted curves; and Δt is the interval time between two consecutive pulse stimuli. Notably, in biological synapses, the values of τ_1 and τ_2 both range from milliseconds to seconds, where the value of τ_1 tends to be an order of magnitude smaller than the value of τ_2 [68,72,81]. Furthermore, it has been reported in the literature that PPF behavior is also influenced by numerous external factors, for instance, the wavelength of the optical stimulus [Figs. 3(f) and 3(g)] [1,55] or the spikes of the electrical stimulus [Fig. 3(h)] [82]. Similarly, the mechanisms of PPF behavior in the neurosynaptic devices are caused by many factors, such as the growing number of conductive ions accumulated at the interface when τ is greater than Δt, allowing the channel conductance to be enhanced with the increase of the pulse number [86].

3. STP to LTP Transition

Depending on the duration of changes in synaptic weight, synaptic plasticity is divided into short-term plasticity (STP), which gradually recovers to its initial state within a short period after being triggered, and long-term plasticity (LTP), which maintains variations in synaptic weight for minutes, weeks, or even permanently [68,72]. The above-mentioned EPSC, IPSC, PPF, and PPD are all typical manifestations of STP, which is stored in the hippocampus of the brain according to the model of learning and memory proposed by Atkinson and Shiffrin [Fig. 4(a)] [87,89]. After a constant process of consolidation and rehearsal, the synaptic weights are strengthened, and STP transforms into LTP for storage in the cerebral cortex

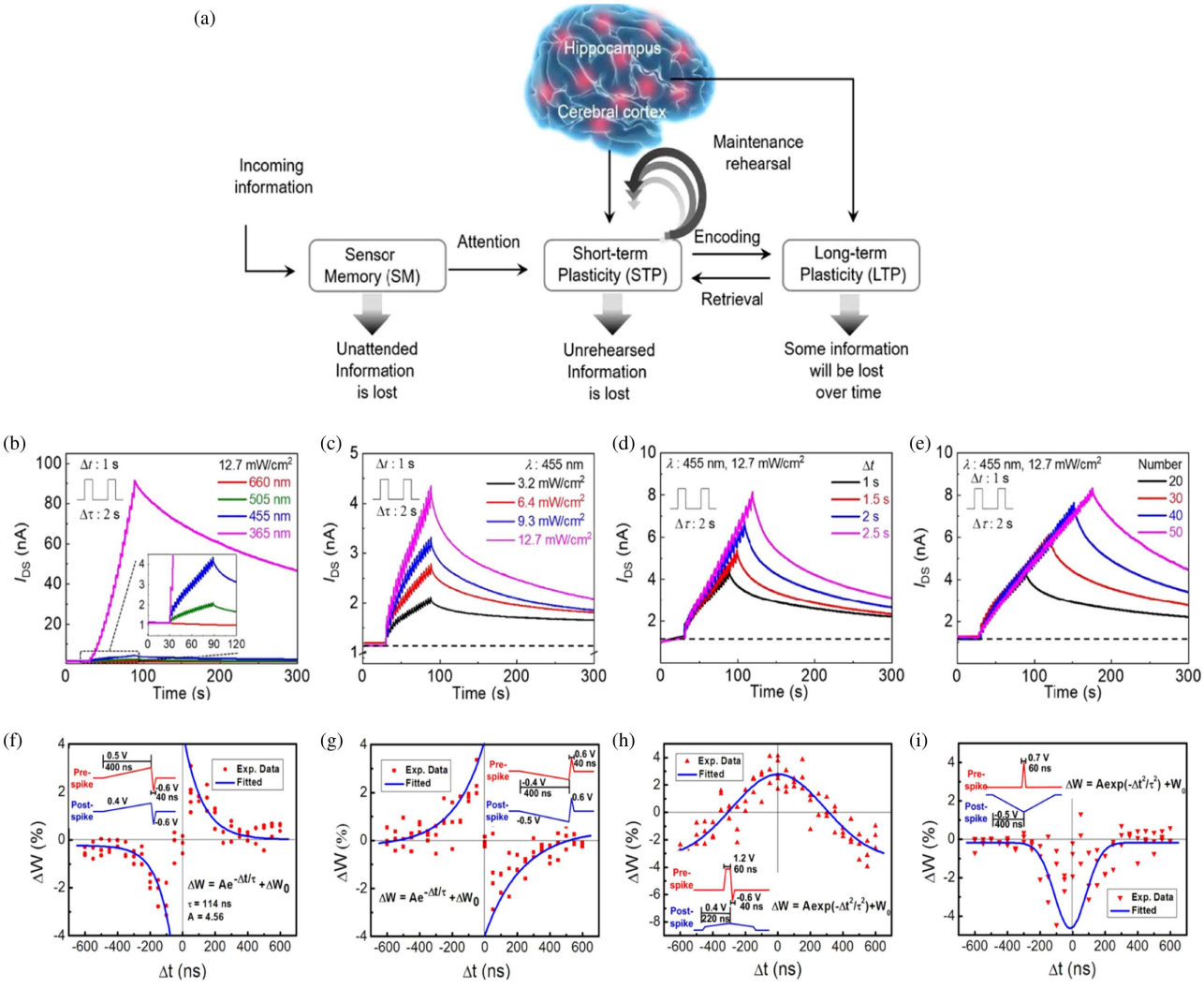

Fig. 4. (a) Schematic diagram of a typical STP to LTP transition model. (b)–(e) I_{ds} as a function of (b) presynaptic optical pulse wavelength, (c) presynaptic optical pulse density, (d) presynaptic optical pulse width, and (e) number of presynaptic optical pulses. (a)–(e) Reprinted with permission from [87]. Copyright 2022, Springer Nature. Four typical STDP learning rules are illustrated in (f) the antisymmetric Hebbian learning rule, (g) antisymmetric anti-Hebbian learning rule, (h) symmetric Hebbian learning rule, and (i) symmetric anti-Hebbian learning rule, simulated by a GST-based memristor. (f)–(i) Reprinted with permission from [88]. Copyright 2013, Nature Portfolio.

[68,89,90]. In the human brain, the STP assumes the responsibility of receiving and transmitting information, while LTP, as a typical representative of Hebb's plasticity, is regarded as the basis for achieving learning and memory functions [91–93]. Referring to Hebb's postulate (this synaptic efficacy improves if the postsynaptic neuron is stimulated successively and repeatedly by the presynaptic neuron) [94,95], the synaptic weight can be adapted by varying the pulse wavelength, power density, pulse width, and number of incident light pulses to implement the transition from STP to LTP further [Figs. 4(b)–4(e)], which is the basis of the learning behavior imitated by synaptic devices [85,87,91,96–98]. Notably, following the enhancement or diminution of synaptic weight, short-term potential (STP) and long-term potential (LTP) are classified as short-term depression (STD) and long-term depression (LTD), respectively [99].

4. Spike-Dependent Plasticity

Spike-dependent plasticity (SDP) is regarded as the dependence of synaptic plasticity on spiking stimuli, with specific manifestations of various types such as synaptic duration-dependent plasticity (SDDP), spike-rate-dependent plasticity (SRDP), synaptic voltage-dependent plasticity (SVDP), and spike-number-dependent plasticity (SNDP), which reflect the implications of the width, frequency, amplitude, and the number of spike pulses transmitted from presynaptic neurons on synaptic weights, respectively [51,90,100–105]. In terms of SRDP, two features of LTP, known as LTP and LTD, are triggered by pulse spikes at high frequency from 20 to 100 Hz and low frequency from 1 to 5 Hz, respectively [93,106].

Similar to SRDP, spike-timing-dependent plasticity (STDP) is one of the representative forms of LTP, which was first initially proposed as the computer learning algorithm widely applied in machine intelligence and now reflects the dependence of synaptic weights (ΔW) on the sequence and time interval (Δt, $\Delta t = t_{\text{post}} - t_{\text{pre}}$) of pre- and postsynaptic neural activities in biological synapses [107–110]. More specifically, when the presynaptic spike arrives ahead of the postsynaptic spike ($\Delta t > 0$, prepost-pairing), the pulse signal induces the generation of LTP, with an increase in synaptic weight; on the contrary, the degree of synaptic connection diminishes at $\Delta t < 0$ (postpre-pairing), and LTD behavior is triggered [92,95,111,112]. Various spiking patterns and relative spike durations influence the direction and amplitude of synapses, inducing the generation of the typical four forms of STDP, namely the antisymmetric Hebbian learning rule, antisymmetric anti-Hebbian learning rule, symmetric Hebbian learning rule, and symmetric anti-Hebbian learning rule, respectively [56,88,94,113,114]. Li *et al.* reported a GST-based memristor synaptic device relying on the capturing and releasing of charge traps caused by defects within the material itself, and four different forms of STDP can be well exhibited by the device, as shown in Figs. 4(f)–4(i) [88]. In computational neuroscience, asymmetric STDP learning rules can be modeled by exponential functions, while symmetric STDP learning rules are fitted by Gaussian functions, which can be summarized as [64,88,93,115]

$$\Delta W = \begin{cases} Ae^{\left(-\frac{\Delta t}{\tau}\right)} + W_0, \text{asymmetric} \\ Ae^{\left(-\frac{\Delta t^2}{\tau^2}\right)} + W_0, \text{symmetric} \end{cases}, \tag{3}$$

where A and W_0 are defined as the scaling factor of the function and the constant indicating the non-associative component for synaptic weight alteration, respectively, and τ is considered as the time constant of the fitted function.

C. Energy Consumption

The energy consumption generated when any synaptic behavior has been triggered is considered one of the essential indicators to evaluate the performance of synaptic devices, and the calculation was proposed by Kuzum *et al.* in 2013 [116]. Specifically, the energy consumption $E = V \times I \times t$, where V is defined as the electrical pulse amplitude, t is defined as the width of the electrical pulse, and I is regarded as the triggered PSC [117]. In contrast to electrical synapses, a new calculation method of energy consumption was introduced by Tan *et al.* for optical synaptic devices: $E = P \times S \times t$, where P is determined as the power density of the incident light pulse, t is defined as the optical pulse width, and S is defined as the effective illumination area of the synaptic device [118]. Remarkably, one of the two energy consumption calculation methods above applies to synaptic events triggered by electrical pulses, while the other focuses on the energy consumption induced by optical pulses. When the synaptic behavior is stimulated by optical and electrical signals in parallel, then the energy consumption is also obtained by superimposing the two calculation methods above [63].

The human brain consumes a fixed amount of energy to carry out the normal physiological activity, and the cost of neuronal release spikes is so prohibitive that only no more than 1% of neurons are active simultaneously [119]. Furthermore, in biological nervous systems, 1–10 fJ energy is consumed per synaptic spike, a metric that can be accomplished by the few synaptic devices proposed in recent years [116,120]. However, the energy consumption of most synaptic devices is quantified in pJ or even nJ, which hinders the development of neuromorphic computing [63,64,121–124]. To achieve large-scale integration of synaptic devices, the limitation of high energy consumption must be overcome, which can be optimized by weakening the programming pulse amplitude, shortening the programming pulse width, decreasing the effective area of the synaptic device, and reducing the programming current, respectively [65,66,125].

3. STRUCTURE AND MECHANISM OF MHP-BASED OPTOELECTRONIC SYNAPTIC DEVICES

To date, significant efforts have been devoted to designing and fabricating MHP-based artificial synaptic devices for achieving synaptic plasticity. According to a different stimulation source, MHP-based optoelectronic synapses can be divided into all-optical stimulated synapses and optically–electrically synergistic stimulated synapses. In this section, we focus on two-terminal memristors and three-terminal transistors employed for artificial optoelectronic synapses, as well as analyzing their device architectures and operational mechanisms. More specifically, the fundamental synaptic characteristics (terminal number, synaptic functions, energy consumption, etc.) are summarized in Table 1.

Table 1. Summary of MHP-Based Optoelectronic Synapses

Device Architectures	Structure	Availability of Stimuli	Operation Mechanism	Synaptic Functions	Energy Consumption	Reference
Au/P(VDF - TrFE)/$Cs_2AgBiBr_6$/ITO	Two-terminal	All-optical	Schottky barrier	STP/SNDP/SRDP	0	[51]
ITO/PEDOT:PSS/CuSCN/$CsPbBr_3$ PNs	Two-terminal	Optical/Electrical	Surface charge trapping/detrapping	STP/LTP	–	[126]
Graphene/h-BN/$CsPbBr_3$ QDs	Three-terminal	Optical/Electrical	Photoelectric effect	STP/LTP	–	[57]
PEA_2SnI_4/Y_6	Three-terminal	All-optical	Surface charge trapping/detrapping	STP/LTP	–	[60]
IGZO/$CsPbBr_3$ QDs	Three-terminal	Optical/Electrical	Surface charge trapping/detrapping	STP/LTP	–	[127]
BA_2PbBr_4/IZTO	Three-terminal	Optical/Electrical	Surface charge trapping/detrapping	STP/LTP	–	[128]
$CsPbBr_3$/TIPS	Three-terminal	Optical/Electrical	Surface charge trapping/detrapping	STP/LTP	0.076 pJ	[62]
BCP/$MAPbBr_3$/PS/pentacene	Three-terminal	Optical/Electrical	Surface charge trapping/detrapping	STP/LTP	–	[129]
Au/KI-$MAPbI_3$/ITO	Two-terminal	Optical/Electrical	Ion migration	STP	–	[130]
IGZO/PVK NPs/IGZO	Three-terminal	Optical/Electrical	Surface charge trapping/detrapping	STP/LTP	–	[131]
$CsPbI_2Br$ PNCs/IGZO	Three-terminal	Optical/Electrical	Persistent photoconductivity (PPC)	STP/LTP	<2.6 pJ	[132]
SiNM/$MAPbI_3$	Three-terminal	All-optical	Surface charge trapping/detrapping	STP/LTP	~1 pJ	[23]
ITO/perovskite/P3HT/Ag	Two-terminal	Optical/Electrical	Ion migration	STP/LTP/STDP	–	[133]
ITO/PCBM/$MAPbI_3$:Si NCs/Spiro-OMeTAD/Au	Two-terminal	All-optical	Surface charge trapping/detrapping	STP/SNDP/SRDP	0	[20]
$CsPbBr_3$ QDs/MoS_2	Three-terminal	Optical/Electrical	Surface charge trapping/detrapping	STP/LTP	4.24 nJ	[58]
$(PEA)_2SnI_4$	Three-terminal	All-optical	Surface charge trapping/detrapping	STP/LTP	–	[134]
$CsBi_3I_{10}$/SWCNTs	Three-terminal	Optical/Electrical	Surface charge trapping/detrapping	STP/LTP	–	[135]
PDVT-10/PVP + $CsPbBr_3$ QDs	Three-terminal	All-optical	PPC effect	STP/LTP	4.1 pJ	[136]
$CsPbBr_3$ QDs/PMMA/pentacene	Three-terminal	Optical/Electrical	Surface charge trapping/detrapping	STP/SVDP/LTP SNDP/SDDP	1.4 nJ	[61]
(rGO/PEDOT:PSS)/$(PEA)_2SnI_4$	Two-terminal	All-optical	Surface charge trapping/detrapping	STP/LTP	–	[137]
$MAPbBr_3$ PDs grown from graphene lattice	Three-terminal	Optical/Electrical	Surface charge trapping/detrapping	STP/LTP	36.75 pJ	[138]
$CsPbBr_3$ QDs/DPP-DTT	Three-terminal	Optical/Electrical	Surface charge trapping/detrapping	STP/LTP	0.4 pJ	[56]
ITO/SnO_2/$CsPbCl_3$/TAPC/TAPC:MoO_3/MoO_3/Ag/MoO_3	Two-terminal	All-optical	Surface charge trapping/detrapping	STP/SFDP/LTP SNDP/SDDP	–	[139]

A. MHP-Based Optoelectronic Synaptic Memristors

1. Optically–Electrically Synergistic Stimulated Optoelectronic Synaptic Memristors

Two-terminal memristors, first proposed by Prof. Chua in 1971 [140], are widely employed in hardware implementation for neural networks due to advantages such as a simple fabrication process, low energy consumption, and large-scale integration [141,142]. Interestingly, for such memristors with inherent switching effects, the transition between multiple resistive states relies on the electrical-bias-history-dependent resistance, a characteristic applicable to simulating synaptic behaviors [143–145]. A typical MHP-based optoelectronic synaptic memristor with an Ag/$MAPbI_3$/Ag horizontal structure was presented by Zhu and Lu [Fig. 5(a)] [76]. As shown in Fig. 5(b), resistance switching (RS) dynamics can be tuned by optical stimulation since illumination inhibits the formation of iodine vacancy (V_I/V_I^*) in $MAPbI_3$ while simultaneously facilitating its spontaneous annihilation process. In addition, the accumulation and spontaneous decay of the concentration in V_I/V_I^* are intimately related to the stimulus of the input pulses, and the $MAPbI_3$-based memristor can mimic synaptic behavior, such as STP and LTP benefiting from the similarity of this dynamics of V_I/V_I^* to Ca^{2+} of biological synapses. Further, the dependence of the spontaneous attenuation rate of the conductance upon illumination and the LTP/LTD behavior of the device is illustrated in

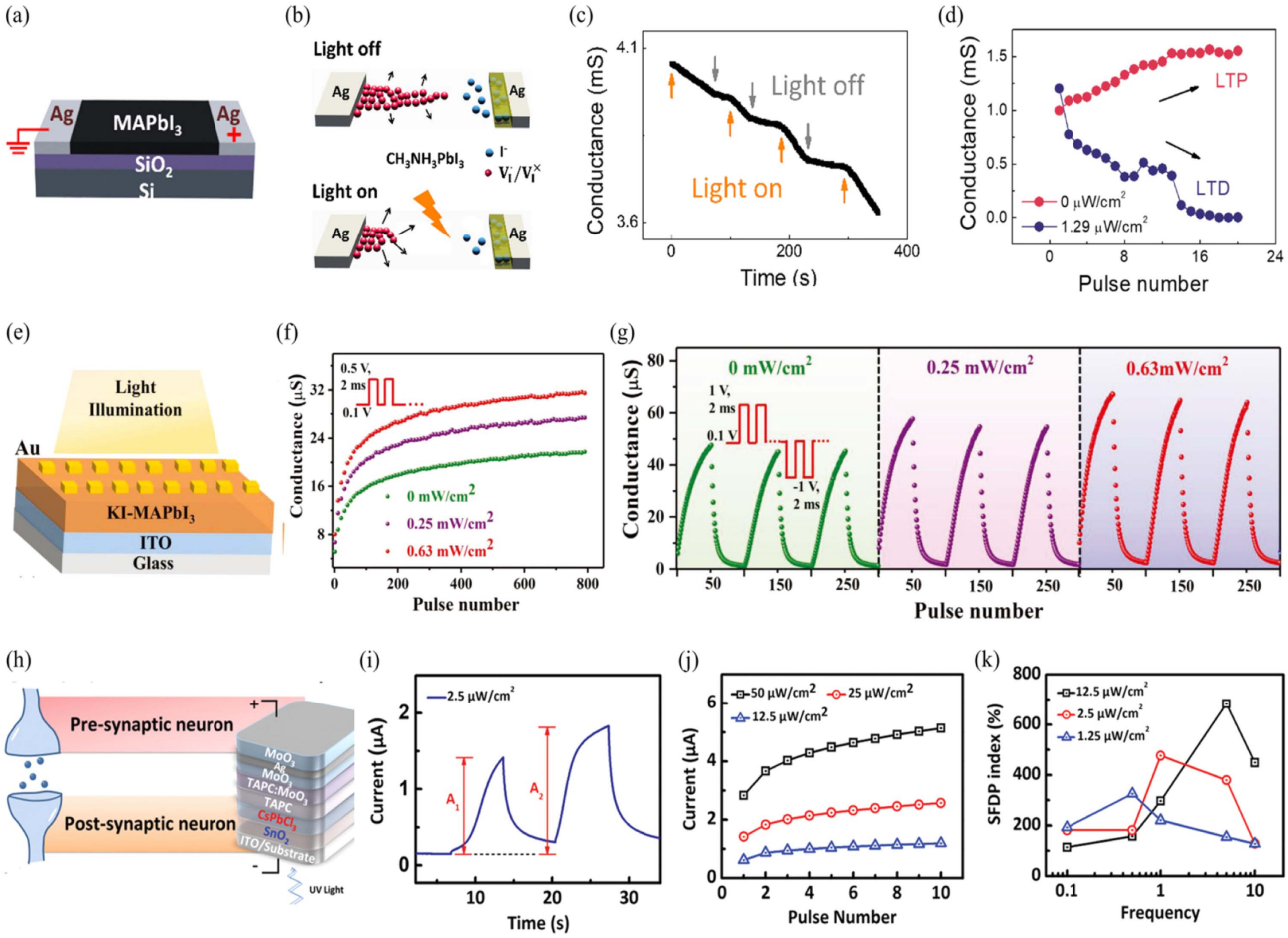

Fig. 5. (a) Schematic illustration of the $MAPbI_3$-based optoelectronic synaptic memristor prefabricated on the SiO_2 substrate. (b) Schematic diagram of the generation/annihilation process of $V_I^{\cdot}/V_I^{*}$ under darkness (upper) and illumination (lower). (c) Dependence of the spontaneous decay of the $MAPbI_3$-based memristor conductance value upon illumination (1.29 $\mu W/cm^2$). (d) LTP/LTD of the $MAPbI_3$-based optoelectronic synapse with applying electrical spikes (1 V, 10 ms) upon darkness/illumination (1.29 $\mu W/cm^2$). (a)–(d) Reprinted with permission from [76]. Copyright 2018, American Chemical Society. (e) Schematic illustration of the Au/KI–$MAPbI_3$/ITO optoelectronic synaptic memristor prefabricated on the glass substrate. (f) Dependence of the device conductance on the electrical stimulus (0.5 V, 2 ms, $V_{read} = 0.1$ V) upon illumination (0, 0.25, 0.63 mW/cm^2). (g) LTP/LTD behaviors of the Au/KI–$MAPbI_3$/ITO-based synapse with applying consecutive positive/negative voltage spikes (1 V/–1 V, 2 ms, $V_{read} = 0.1$ V) at various illumination intensities. (e)–(g) Reprinted with permission from [130]. Copyright 2021, Wiley-VCH. (h) Schematic illustration of the ITO/SnO_2/$CsPbCl_3$/TAPC/TAPC:MoO_3/MoO_3/Ag/MoO_3 synaptic memristor with dual-mode operation. (i) EPSC triggered by two successive optical spikes (2.5 $\mu W/cm^2$, 365 nm). (j) Dependence of the PSC on the pulse number upon various illumination intensities (from 12.5 to 50 $\mu W/cm^2$). (k) Dependence of the SFDP index on the various illumination intensities ranging from 1.25 to 12.5 $\mu W/cm^2$. (h)–(k) Reprinted with permission from [139]. Copyright 2021, Wiley-VCH.

Figs. 5(c) and 5(d), implying that the synaptic behaviors of the $MAPbI_3$-based memristor are synergistically regulated by the optical and electrical stimuli. Recently, the Au/KI-$MAPbI_3$/ITO optoelectronic synaptic memristor with vertical structure was proposed by Lao *et al.* utilizing the excellent optical properties of $MAPbI_3$ [130]. The device architecture is shown in Fig. 5(e), where the additive KI was introduced to enhance the crystallinity of $MAPbI_3$ while modifying its surface defects, which facilitated the ion migration of the mixed film, in turn leading to the dynamic range of the memristor conductance being further extended. In this case, the conductance level initially increases sharply after the application of 800 consecutive voltage pulses followed by a steady level to the maximum value, while the conductance relies on the illumination assuming a synergistic stimulus role, meaning that the memory level of the electrical input is enhanced upon illumination [Fig. 5(f)]. Further, the classical LTP and LTD behaviors triggered by the voltage stimuli applied under illumination were observed [Fig. 5(g)].

2. All-Optical Stimulated MHP-Based SPTs

Compared with conventional electrically driven synaptic devices, light-driven synapses have attracted much attention due to lower interconnection energy consumption, faster signal transmission, and higher bandwidth [29]. Given this, Yang *et al.* demonstrated an all-optical two-terminal synaptic memristor with an ITO/SnO_2/$CsPbCl_3$/TAPC/TAPC:MoO_3/MoO_3/Ag/MoO_3 vertical structure [Fig. 5(h)] [139], where the TAPC layer serves as a hole transporting layer and the $CsPbCl_3$ film layer assumes the responsibility of a UV light absorber.

Eventually, based on the working mechanism of UV-induced surface charge trapping/detrapping under the stimulus of optical spikes, this dual-mode tuned all-optical synapse can well accomplish biological synaptic behaviors such as PPF, SNDP, and SFDP [Figs. 5(i)–5(k)].

B. MHP-Based Synapse Phototransistors

1. Optically–Electrically Synergistic Stimulated MHP-Based SPTs

Unlike two-terminal memristors, three-terminal transistors have multi-gate structures comparable to biological dendrites, facilitating synergistic modulation of input pulses, stability of operation, and the transmission of synaptic signals [139,146–148]. Emerging MHP-based synapse phototransistors (SPTs) have attracted attention due to their outstanding photovoltaic conversion efficiency, further demonstrating their structural stability and operational controllability. For instance, Park *et al.* have designed an ITZO/BA_2PbBr_4 SPT for NVSs with the structure shown in Fig. 6(a), which regulates synaptic behaviors by coupling stimulation with optical and electrical spikes [128]. When the light signal was applied to the BA_2PbBr_4-based SPT, the photogating effect was induced due to the regulation of the energy band at the interface between ITZO and BA_2PbBr_4 facilitating the separation of photo-excited carriers, thereby increasing the value of PSC by capacitive coupling [Fig. 6(b)]. Additionally, the characteristics of LTP and LTD were observed, which are generated by the photogating effect triggered by 50 successive light pulses (100 μW/cm^2, 1 s) and the recombination of photo-excited carriers prompted by 50 successive positive gate pulses (20 V, 2 s) [Fig. 6(c)]. Notably, the value of EPSCs in LTP characteristics increased with the decay of λ, following the optical absorption spectra of the BA_2PbBr_4 film. Not only the gate voltage pulses but also the drain electrical spikes of the SPTs are available for the regulation of the conductance state as demonstrated in a graphene-PQD (G-PQD) superstructure exploited by Pradhan *et al.* [138]. The current-voltage characteristic of the proposed structure with and without illumination is shown in Fig. 6(d), where quantum dots act as the photoabsorbing material and graphene assumes the responsibility of an effective carrier transport channel. The behaviors of LTP and LTD can be achieved as band-to-band/impurity-to-band transitions in the SPT prompting an effective charge transfer from PQDs to the graphene layer. Moreover, the study briefly

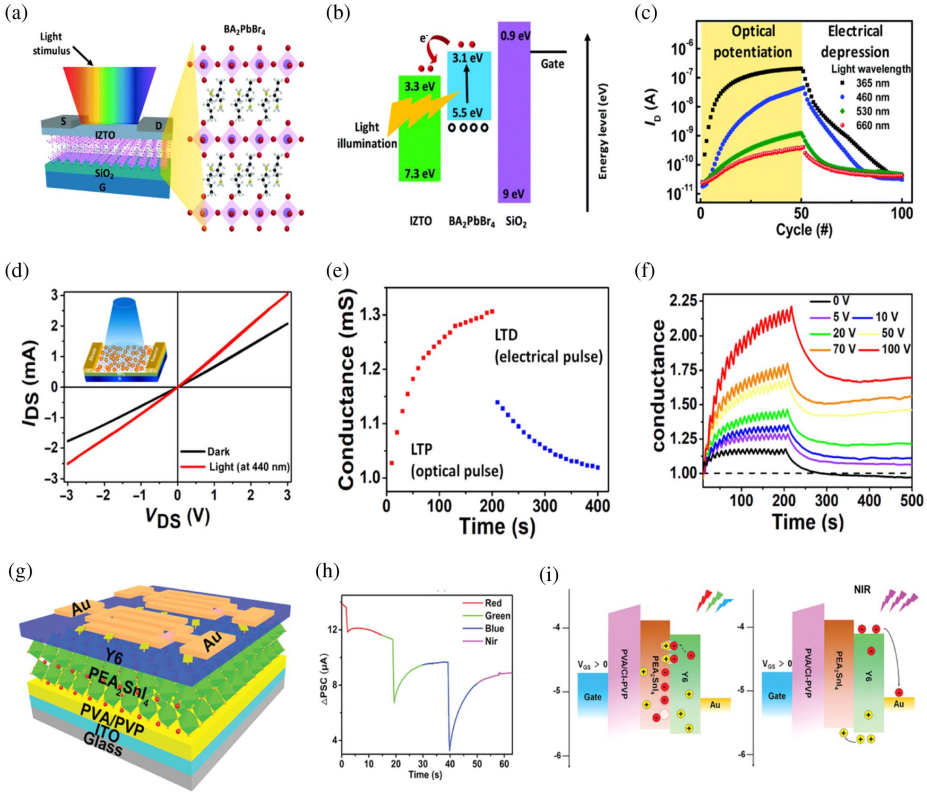

Fig. 6. (a) Schematic illustrations of the BA_2PbBr_4-based SPT by inserting the IZTO layer. (b) Energy band diagram of the ITZO/BA_2PbBr_4 SPT under illumination. (a), (b) Reprinted with permission from [128]. Copyright 2021, Royal Society of Chemistry. (c) LTP and LTD of the ITZO/BA_2PbBr_4 SPT with applying 50 potentiation (100 μW/cm^2, 1 s) light pulses and 50 depression (20 V, 2 s) gate pulses. Adapted with permission from [128]. Copyright 2021, Royal Society of Chemistry. (d) The I_{DS} – V_{DS} characteristic of the G-PQD SPT was evaluated under illumination and dark, respectively. Inset, schematic illustrations of the SPT based on G-PQD superstructure. (e) LTP and LTD of the G-PQD SPT with applying 20 consecutive potentiation (1.1 μW/cm^2, 5 s) light spikes and consecutive depression (–0.5 V, 1 s) drain spikes. (f) LTP of the G-PQD SPT stimulated by 20 consecutive light spikes (1.1 μW/cm^2, 5 s) with different V_G. (d)–(f) Reprinted with permission from [138]. Copyright 2021, American Association for the Advancement of Science. (g) Schematic illustration of the PEA_2SnI_4/Y_6 ambipolar SPT. (h) Wavelength-dependent ΔEPSC peaks. (i) Operation mechanism of synaptic plasticity in response to visible and NIR light pulse irritation. (g)–(i) Reprinted with permission from [60]. Copyright 2021, Wiley-VCH.

analyzed the gate-dependent LTP transient characteristic of the G-PQD SPT stimulated by 20 consecutive light spikes (1.1 μW/cm^2, 5 s) [Fig. 6(f)].

2. All-Optical Stimulated MHP-Based SPTs

Huang *et al.* broadened the absorption spectrum of PEA_2SnI_4 perovskite by inserting a Y_6 organic film, enabling the proposed PEA_2SnI_4/Y_6 ambipolar SPT to actualize the red/green/blue/near-infrared (NIR) wavelength selectivity [60]. With the structure illustrated in Fig. 6(g), this SPT accomplishes synaptic plasticity behaviors in response to stimuli of optical spikes, relying on charge trapping/detrapping processes at the PEA_2SnI_4/Y_6 interface. Compared with the optically–electrically synergistic stimulated devices, as an all-optical type device, the advantage of this structure is that the increase and decrease of conductance can be modulated by the optical signal only, contributing to avoiding the generation of joule heat during the operation. In this work, an IPSC/EPSC was triggered when the SPT was stimulated by a visible/NIR light spike [Fig. 6(h)], with the mechanism of operation shown in Fig. 6(i). Here, electron–hole pairs were generated in both the PEA_2SnI_4 film and Y6 under the stimulus of visible optical spikes, where photogenerated electrons were trapped by Sn vacancies present in the PEA_2SnI_4, which resulted in an enhanced photogating effect and evoked more holes to recombine with partial electrons in the channel, leading to a reduction in the electron concentration and PSC values of the SPT eventually. As opposed to this, when an NIR light spike was applied, benefiting from the generation of electron–hole pairs in Y_6, the holes outflowing from Y_6 were trapped at the PEA_2SnI_4/Y_6 interface, which further contributed to the increase in the values of the PSCs.

4. EMERGING APPLICATIONS

Recently, MHP-based optoelectronic synaptic devices have succeeded in mimicking the basic synaptic functions by skillfully incorporating light as the pulse signal, which builds a bridge to construct AI and brain-like computing at the physical level. Further, this section summarizes the novel application perspectives of the devices and classifies them roughly into three key categories: (i) neuromorphic computing, (ii) high-order learning behaviors, and (iii) NVSs.

A. Neuromorphic Computing

1. Arithmetic Computing

Due to the increasing demand for storage and computational accuracy, most resistive random-access memories (RRAMs) that specialize in binary storage face the challenge of insufficient reproducibility, attracting attention to innovative computational concepts [2,149–151]. In fact, since the increased/decreased MHP-based optoelectronic device currents in response to optical/electrical impulses strongly resemble the addition/subtraction calculation of the abacus, the proposed MHP-based optoelectronic synaptic devices on this basis can serve to accomplish decimal arithmetic functions, which have implications for the implementation of algorithms other than binary [152–154]. Huang *et al.* reported the MHP-based optoelectronic memristor with $MAPbI_3$/SiNCs hybrid film fabricated by a two-step method in 2020 [20]. Figure 7(a) illustrates the increase of the initial current (EPSC*i*) as a function of the stimulus number (*i*) of the device under optical spikes irritation (with interval time of 0.2 s). In general, a perfect linear correlation has to be exhibited between *i* and ESPC*i* to satisfy the arithmetic requirement of decimal counting (here, the linear fitting Pearson correlation coefficient is up to 0.99) [155]. When $m + n$ is calculated, the value of *i* is derived by matching the exciting current value with the specific EPSC*i* by adding *n* consecutive pulse stimuli after *m* consecutive pulse stimuli. The operation of subtraction works in the same way as addition [151], and the value of $m - n$ can be calculated by computing the amount of optical excitation necessary for the EPSC*i* change from EPSC*n* to EPSC*m* [Fig. 7(b)]. In the case

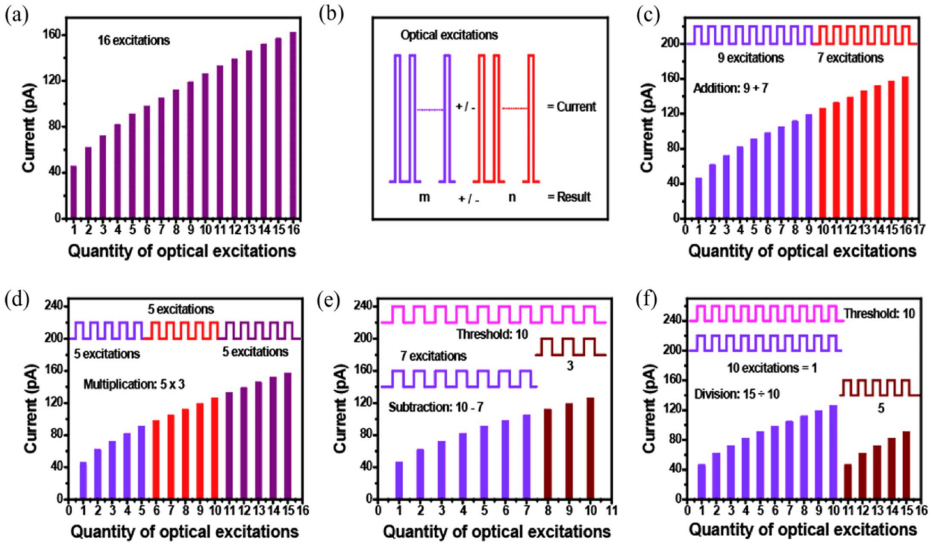

Fig. 7. (a) Excitation currents (EPSC*i*) by optical pulses are a linear function over the number of optical impulses (*i*, ranging from 1 to 16). (b) Schematic diagram of the principle for employing optical excitation in a synaptic device to achieve addition and subtraction operations. Diagram of the (c) addition operation "9 + 7," (d) multiplication operation "5 × 3," (e) subtraction operation "10 – 7," and (f) division operation "15/10". Reprinted with permission from [20]. Copyright 2020, Elsevier.

of "9 + 7," the EPSC excited by 9 plus 7 consecutive optical pulses reaches 162 pA, which equals the value of EPSC16, corresponding to the calculation process of "9 + 7" = 16 [Fig. 7(c)]. Apart from simple addition algorithm, the operation of subtraction, multiplication, and division can also be implemented by these MHP-based synaptic devices, as shown in [Figs. 7(d)–7(f)].

2. Logic Functions

As is well known, not only arithmetic computation but also dynamic logic operations play an important role in reflecting the data processing capability of the neural system [150], providing additional support for achieving multifunctional neuromorphic computing [154,156,157]. Based on multiple-light-stimulated synapse of DPPDTT/$CsPbBr_3$ QDs with the capability of mimicking essential synaptic behavior [Fig. 8(a)], two series of optical signals at 450 and 500 nm were employed by Hao *et al.* to implement Boolean logic arithmetic including both "AND" and "OR" logic functions [158]. Much more interestingly, at a weak optical illumination of 0.12 mW/cm^2, the ΔEPSC value increases beyond a threshold current (5 nA) only when two peaks are imposed on the synapse separately, illustrating the "AND" logic function [Fig. 8(b)]. Nevertheless, with an increased irradiation density of 0.3 mW/cm^2, the ΔEPSC triggered by either stimulus remains high compared to the threshold current, signifying the implementation of the "OR" logic function [Fig. 8(c)].

In addition to simple "AND" and "OR" logic operations, other dynamic logical functions such as the nervous system's ability to process information can be embodied by MHP-based optoelectronic synaptic devices [53,136]. For example, Zhang *et al.* exploited optoelectronic transistors to achieve synaptic functions [Fig. 8(d)] [56], in which the $CsPbBr_3$ QDs/DPP-DTT heterostructure facilitates photonic modulation, while the electrical modulation arises from the electric double layer effect in the ionic conductive cellulose nanopaper (ICCN). Here, electrical and optical signals work in tandem to control the switching of logical functions during equipment operation. The output current is above the threshold value (−60 pA) only when two electrical spikes (−0.5 V) are stimulated simultaneously without light modulation, corresponding to the "AND" logic function [Fig. 8(e)], while the current triggered independently by any electrical spike exceeds the threshold current when modulated by weak light and is considered as the "OR" logic operation [Fig. 8(f)]. Further, the "NAND" logic operation

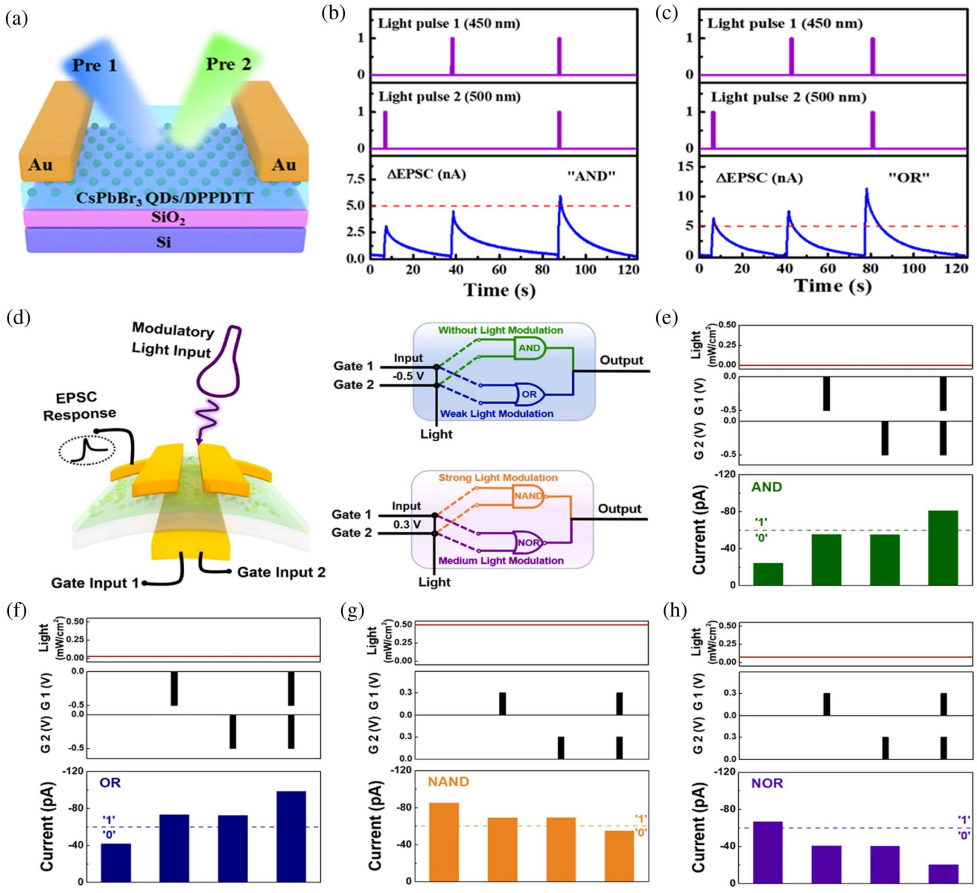

Fig. 8. (a) Schematic illustration of the multi-input light-stimulated $CsPbBr_3$ QDs-based optoelectronic synaptic transistor. Diagram of the (b) "AND" and (c) "OR" logic functions tuned by multiple optical inputs. (a)–(c) Reprinted with permission from [158]. Copyright 2020, American Chemical Society. (d) Schematic diagram of a synapse for switching logic functions via electrical and optical signals. Input-output characteristics of the (e) "AND," (f) "OR," (g) "NAND," and (h) "NOR" logic operations moderated synergistically by the optical and electrical inputs. (d)–(h) Reprinted with permission from [56]. Copyright 2022, Elsevier.

modulated by medium light is proposed when both electrical spikes added to the gate electrode are 0.3 V [Fig. 8(g)], and the "NOR" logic operation is induced by raising the light intensity to strong light [Fig. 8(h)].

3. Artificial Neural Networks

It is well known that brain-inspired neuromorphic computing breaks the limitations of computing speed, while the emergence of novel synapse-based ANNs provides the potential to render their terminal form [56,159,160]. Han *et al.* designed a light-stimulated synaptic transistor device based on a graphene/hexagonal boron nitride (h-BN)/perovskite QD structure and then investigated the learning capability of the device through the Modified National Institute of Standards and Technology (MNIST) database [57]. As shown in Figs. 9(a) and 9(b), the device was stimulated with 100 continuous light pulses and 100 continuous electrical pulses to obtain 200 conductance values, which were used as synaptic weights by the researchers to construct a supervised learning framework for ANN; 784 input neurons, 300 hidden neurons, and 10 output neurons were linked by synaptic weights to form the ANN [Fig. 9(d)]. The recognition accuracy of the device-based ANN gradually saturates with the amount of training, and when tested with handwritten digit images from the MINIST dataset, the overall recognition accuracy of up to 91.5% can be seen at around 40 training epochs [Fig. 9(c)]. The authors then directly demonstrate the superior recognition ability of the ANN by showing the weight mapping matrix of the output images. As shown in Figs. 9(e) and 9(f), the originally ambiguous outlines eventually present the numbers clearly after continuous training, which shows that the ANN has excellent pattern recognition ability and provides another possibility for the development of neuromorphic computing.

B. High-Order Learning Behaviors

1. STDP

As a fundamental characteristic of event-driven learning in neural network systems [161], STDP learning rules are increasingly proposed as a basis for neuromorphic modeling built on CMOS circuits or memristor synapses [56,162–169]. Yang *et al.* proposed a synaptic memory with an ITO/CsPbBr2I/P3HT/Ag structure, which benefited from the migration properties of halogen ions and succeeded in imitating the STDP behavior of synapses [133]. As shown in Fig. 10(a), a series of presynaptic pulses (V_{pre}, amplitude of 0.7 V) and postsynaptic pulses (V_{post}, amplitude of −0.3 V) with a pulse width of 1 s were applied to the Ag electrode and ITO electrode at both terminals of the memristor, respectively. Here, synaptic weights (ΔW) reach a maximum when both V_{pre} and V_{post} arrive at the same time, followed by a decline with increased time interval (Δt), denoted as the symmetric Hebbian learning rule [Fig. 10(b)]. When reversed spike V_{pre} (amplitude of −0.7 V) and V_{post} (amplitude of 0.3 V) stimuli are applied to the memristor, the synaptic weights change from excitatory to inhibitory previously, also diminishing reliance on the increasing Δt, and in this way, the symmetric anti-Hebbian learning rule is observed [Fig. 10(c)]. In biological systems, the majority of the information is available through vision. As well for synaptic devices, the introduction of optical pulses as stimulus signals to mimic STDP holds enormous promise apart from electrical pulse activation. In Fig. 10(d), silicon solar cells are connected in series with the ITO electrode and Ag electrode of the memristor for constituting the artificial retina system. During the operation of the device, the photovoltaic cell generated electrical spikes upon two sets of optical pulses, which corresponded to the V_{pre} (amplitude of 50 mA/cm^2, width of 30 s) and V_{post} applied to the ITO and Ag electrodes, respectively. For the solar

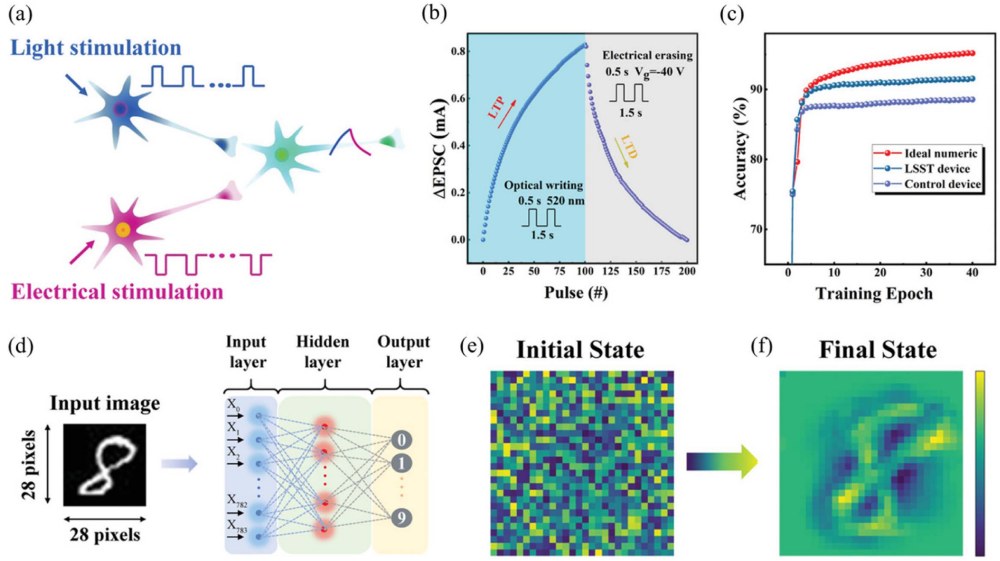

Fig. 9. (a) Schematic illustration of the changes in postsynaptic currents resulting from successive stimulation with optical and electrical signals. (b) Characteristic curves of optical pulse writing and electrical pulse erasing of the device. (c) Variation curves of handwritten digit recognition accuracy along with training epochs of different devices. (d) Schematic illustration of input number "8" and artificial neural network. (e) The initial state of the weight matrix is related to the input numbers. (f) The final state of the weight matrix is related to the input numbers. Reprinted with permission from [57]. Copyright 2022, Wiley-VCH.

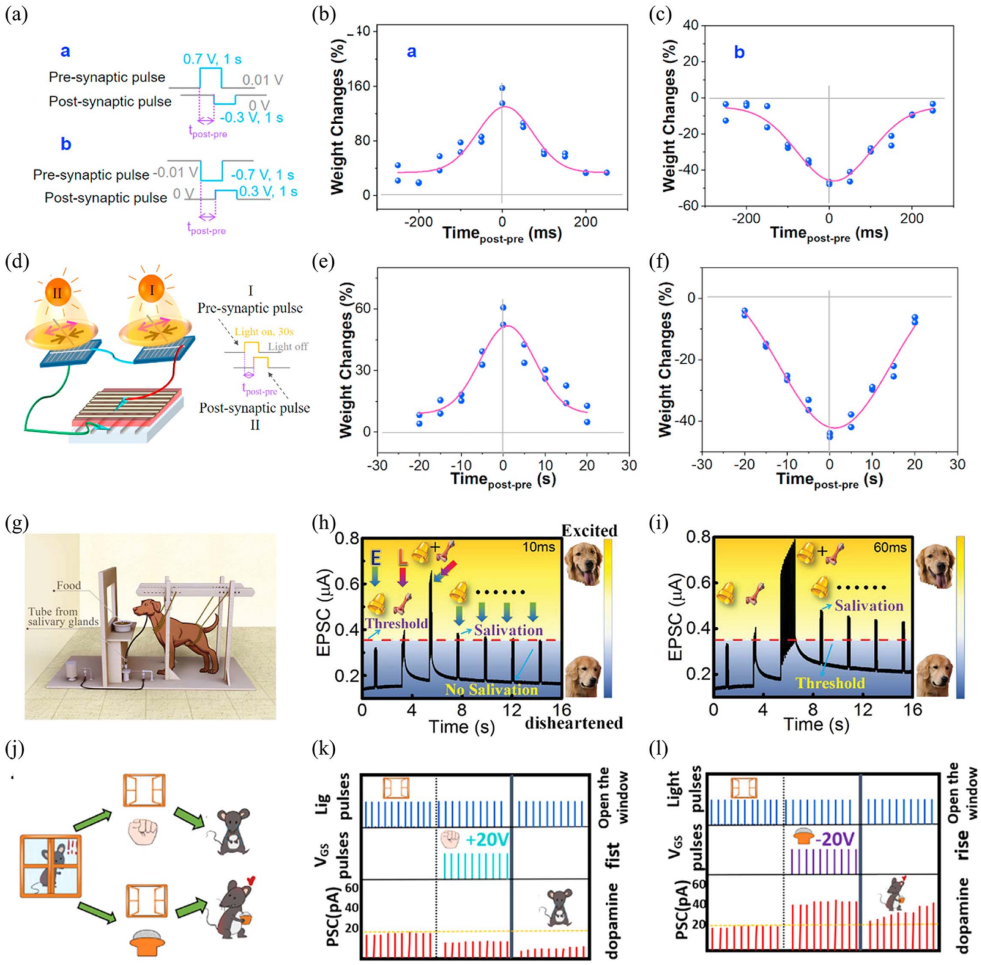

Fig. 10. (a) V_{pre} and V_{post} applied to perovskite-based memristors evoked both (b) the symmetric Hebbian learning rule and (c) the symmetric anti-Hebbian learning rule. (d) V_{pre} and V_{post} applied to a memristor-based artificial retinal system evoked both (e) the symmetric Hebbian learning rule and (f) the symmetric anti-Hebbian learning rule. (a)–(f) Reprinted with permission from [161]. Copyright 2017, Nature Portfolio. (g) Schematic diagram of the concept of Pavlovian conditioned reflex. (h) Emulation of Pavlovian conditioned reflex by using $CsPbBr_3$–QDs/MoS_2 MVVH. (i) Emulation of Pavlovian conditioned reflex by setting photoelectric synergy training duration to 60 ms. (g)–(i) Reprinted with permission from [58]. Copyright 2020, Wiley-VCH. (j) Schematic diagram of the reward and punishment mechanisms that occur in creatures. (k) Emulation of punishment mechanism by synergistic control of optical spikes and positive voltage spikes. (l) Emulation of reward mechanism by synergistic control of optical spikes and negative voltage spikes. (j)–(l) Reprinted with permission from [131]. Copyright 2021, American Chemical Society.

cell, if the anode and cathode are connected to the ITO electrode and the Ag electrode, ΔW will be decreased with the increased Δt between the two sets of light optical pulses, and the symmetric Hebbian learning rule will be demonstrated [Fig. 10(e)]. In turn, when the cathode and anode of the solar cell were connected to Ag and ITO electrodes, respectively, the inhibitory ΔW attenuated depended on the growing Δt as well, implementing the symmetric anti-Hebbian learning rule [Fig. 10(f)].

2. Associative Learning

Associative learning refers to the influence of the relationships between different events on the brain's learning, inspired by the brain's associations [170,171]. Pavlov's dog experiment, also known as the Pavlovian conditioned reflex, first proposed in 1927, has been simulated by many synaptic devices as a classic case of associative learning [53,130,136,172–175]. Cheng *et al.* reported a phototransistor based on the $CsPbBr_3$ – QDs/MoS_2 mixed-dimensional vertical van der Waals heterojunction (MVVH), which can mimic classical conditioning utilizing photoelectronic hybrid inputs [58]. Herein, food and bell ringing are identified as an unconditioned stimulus (US) and neutral stimulus (NS), respectively, while salivation is defined as an unconditioned response (UR). At first, the UR could be activated by the US alone, but after repeated stimulation by forming an association between US and NS, a separate NS can activate UR, which means that the NS is transformed into a conditioned stimulus (CS) [Fig. 10(g)] [58]. The specific experimental procedure is shown in Fig. 10(h), where 10 consecutive electrical spikes (amplitude of 0.13 V, width of 10 ms) and optical spikes (amplitude of 225 mW/cm^2, width of 10 ms) are employed to simulate NS and US, respectively. Herein, the EPSCs triggered by the electrical pulse stimulus

individually failed to reach the threshold current (I_{TH}), implicating that the dog was unable to generate salivation. After 10 optical and electrical pulse stimuli were applied in parallel, the EPSCs were found to exceed I_{TH} when stimuli with electrical pulses were imposed alone, meaning that the synergetic training conferred the ability to induce conditioned response (CR) in NS. Finally, the EPSC gradually decayed to the original state after a period of US, which indicates the disappearance of the association between US and NS, corresponding to the elimination of redundant information in the human brain [176,177]. Moreover, the triggered EPSCs were significantly increased by increasing the photoelectric synergy training time, as shown in Fig. 10(i), reflecting the fact that, in the case of associative learning, the degree of learning and memory is influenced by the intensity of training. As a further manifestation of associative learning, the reward and punishment mechanism refers to the fact that creatures can be trained by reward and punishment to seek benefits and avoid harm when making decisions. Duan *et al.* introduced IGZO/PVK NPs/IGZO heterostructure-based synaptic devices to mimic the photoelectric-synergistically typical reward and punishment mechanism [Fig. 10(j)] [131]. In this case, opening windows (NS), feeding (reward), and punishment are simulated by optical pulses, negative voltage pulses, and positive voltage pulses, respectively. As a result, after synergistic training with NS and punishment/reward, the triggered EPSCs (biological responses) remained below/above the threshold value even when the punishment/reward behavior was applied individually [Figs. 10(k) and 10(l)].

3. Emotions and Learning

It is well known that emotion, as an emotional experience or response, plays a critical role in learning effectiveness; however, the complex feedback mechanism linking learning and emotion has not been completely elucidated by any research [178–180]. In recent years, emulating this biological behavior with synaptic devices has attracted the interest of researchers [181–183]. Yin *et al.* reported a SiNM/$MAPbI_3$ heterostructure-based optoelectronic synapse that simulates visual learning and memory behaviors, depending on various emotional states [23]. As shown in Fig. 11(a), 30 consecutive optical pulses (wavelength of 532 nm, amplitude of 1 μW/cm^2, width of 200 ms) are applied to the synaptic device acting as the learning process, while a maximum value of the triggered EPSC is defined as the learning result, and the decay of EPSC over time is considered as the forgetting process [Fig. 11(b)]. Further, the positive, neutral, and negative moods correspond to the situations when the gate voltage is equal to −4 V, −3 V, and 1 V, respectively. As a result, the process of learning training for the letter "H" in three different mood states is shown in Fig. 11(c). When people learn with positive moods, the impression of the letter "H" is clearest as well as the most effective; as the mood state turns from neutral to negative, the impression of the letter "H" also changes from general to ambiguous, with weaker learning effects. Notably, the retention of memory after tens of seconds under different moods is similar to the above. In addition to electrical signals, optical signals can also be employed to mimic mood states. For example, Lao *et al.* demonstrated a device based on the Au/KI – $MAPbI_3$/ITO vertical structure by inserting potassium iodide (KI) into $MAPbI_3$ film, which can mimic the learning and memory behaviors that occur when the brain is exposed to positive/negative mood states [130]. Dark states (illumination states) are treated as negative mood (positive mood), while conductance reaching 29 μS is set as the target memory level [Fig. 11(d)]. When the brain is in a negative mood, the value of conductance triggered by 100 consecutive electrical spikes (amplitude of 1 V, width of 2 ms) reaches 29 μS, which is much larger than that required when the brain is in a positive mood. Through a few seconds of the forgetting process, the conductance values have to be stimulated by 58 (13) consecutive electrical spikes to attain 29 μS again when

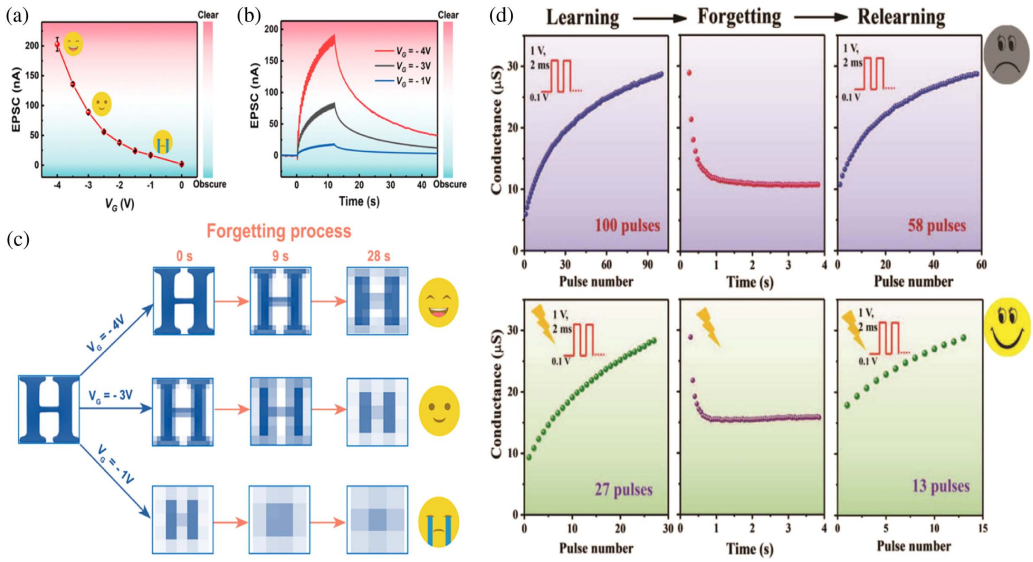

Fig. 11. (a) Relationship between the maximum EPSC triggered by 30 light pulses and varying gate voltages. (b) EPSC is triggered by 30 light pulses at varying gate voltages. (c) Recognition of the letter "H" as the brain enters positive/neutral/negative mood states. (a)–(c) Reprinted with permission from [23]. Copyright 2020, American Chemical Society. (d) Diagram of the relationship between learning and memory under different emotional states. Reprinted with permission from [130]. Copyright 2021, Wiley-VCH.

the brain is in a negative (positive) mood, which means the efficiencies of learning and relearning are controlled by emotions.

C. Neuromorphic Visual Systems

More recently, an extensive number of MHP-based optoelectronic synaptic devices, including MHP-based memristors and MHP-based transistors, were employed to fabricate and mimic artificial intelligence visual systems (AIVs) for sensing and processing images [52,62,67,128,184–186]. As an example, Lee *et al.* reported a dynamic artificial visual adaptation neuron (DAVAN) device with a 3 × 3 array that mimics the perceptual ability of the human brain using the adaptive ability of the device to the incident light intensity, offering the possibility of constructing an artificial neuromorphic device [59]. A schematic diagram of the human visual system is shown in Fig. 12(a), in which nerve cells in the visual cortex perceive and process the visual information delivered by photoreceptors. As shown in Fig. 12(b), after being repeatedly stimulated, biological nerve cells produce a biological habituation process: the facilitation process (pre) and the inhibition process (post), respectively. To mimic this function, the authors proposed an optoelectronic neuromorphic circuit structured by two neurotransistors and a perovskite photodetector [Fig. 12(c)]. The EPSC of the DAVAN device under the stimulation of repeated light pulses is shown in Fig. 12(d). It can be seen that the dynamic trend of the response current is consistent with the biological habituation process in Fig. 12(b). Figures 12(e)–12(h)

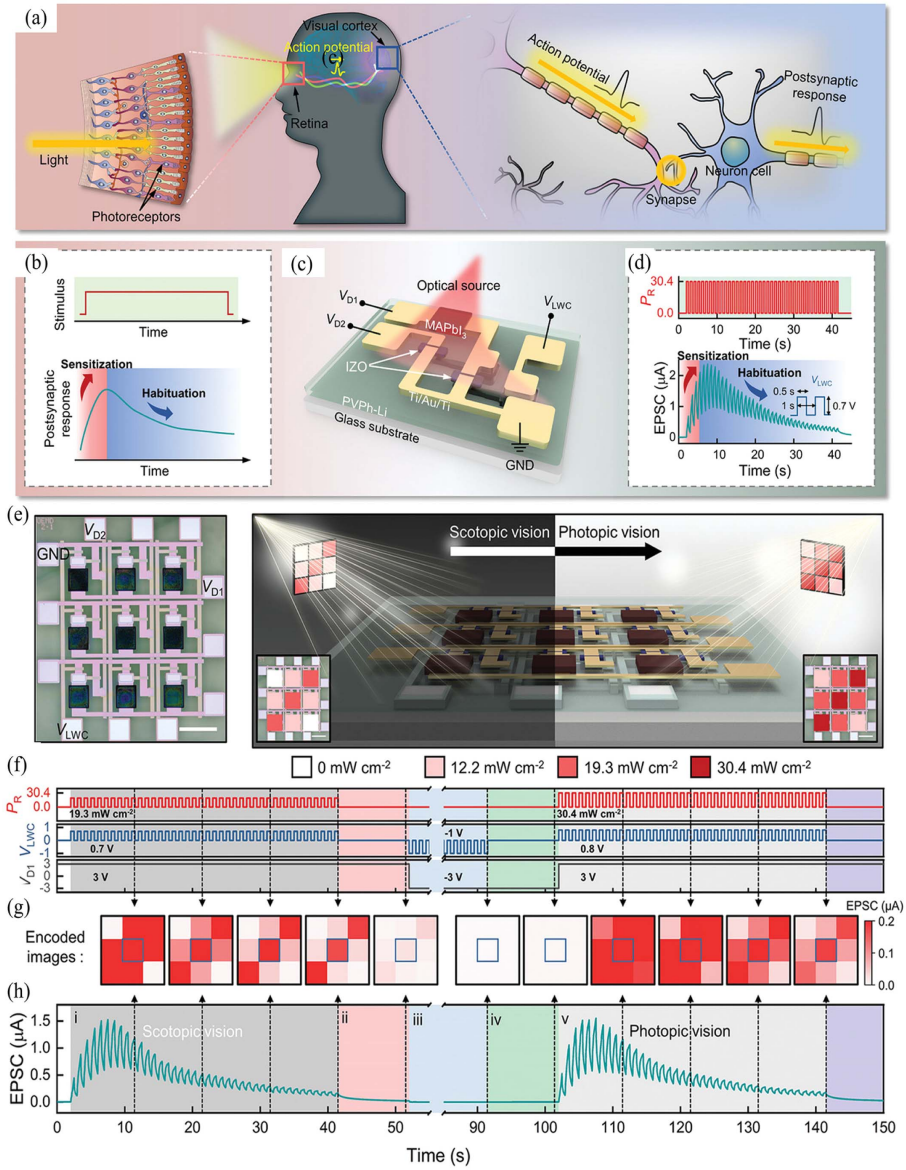

Fig. 12. (a) Schematic diagram of the human visual system. (b) Schematic representation of habituated behavior when the nervous system is stimulated. (c) Schematic diagram of the structure of the DAVAN device. (d) Habituation behavior of the device when stimulated by 40 light pulses. (e) Optical photograph of the DAVAN device for the 3 × 3 array. (f) Schematic diagram of the DAVAN device array in photopic vision condition (left) and scotopic vision condition (right) when illuminated with different intensities of incident light. (g) and (h) Schematic diagram of the dynamic response process of the DAVAN device at the center of the array. Reprinted with permission from [59]. Copyright 2020, Wiley-VCH.

illustrate the optical image and dynamic response process of the 3 × 3 array based on the DAVAN device. Here, the authors successively applied repetitive weak and strong light signal stimuli to the array to simulate the dynamic response EPSC of the array under the photopic vision and scotopic vision conditions. The results show that the device can realize the simulation of the perceptual process of the visual system under different lighting conditions, which has a promising application in the realization of artificial perception systems.

5. CONCLUSION AND PROSPECTS

In this review, recent advances in MHP-based optoelectronic synapses with related neuromorphic applications are summarized. Compared with conventional electrical synapses, optoelectronic synaptic devices using synergistic stimulation exhibit unique superiorities such as higher interference immunity and lower energy consumption, which show promise to break the von Neumann bottleneck and build complex neural networks. So far, benefiting from the fascinating properties of MHPs including charge trap, tunable bandgap, and ion migration, MHP-based phototransistors and memristors have been proposed as optoelectronic synaptic devices. The light-stimulated synaptic plasticity (e.g., PPF, STP, STD, LTP, and LTD) of biological synapses and classical Hebbian learning rules was successfully simulated. In addition, several applications of optoelectronic synapses in the fields of neuromorphic computing, higher-order learning, and AVSs were enumerated, which have significant implications for building energy-efficient neuromorphic systems. Although considerable progress has been achieved on the device architectures and applications of MHP-based optoelectronic synapses, there are still various issues worth further exploration.

(i) Reducing power consumption. In 2016, the power consumption of Google's AlphaGo during the confrontation with a human chess player reached 100 kW, far more than the 20 W consumed by the human brain [187–189]. To the best of our knowledge, optoelectronic synapses with low-power characteristics still require operation consumption in pJ or even nJ per synaptic behavior, leading to an urgent and thorny problem of minimizing energy consumption during large-scale array integration. In this case, downscaling the dimensions of the MHP-based optoelectronic synapses while optimizing their structure is regarded as the effective solution proposed so far.

(ii) All-optical stimulated synapse. Scientific findings show that human access to external information relies on the biological perception system, and the amount of information transmitted by the human visual system accounts for more than 70% [190,191]. For this reason, light signals for constructing optoelectronic neuromimetic engineering have been introduced into synaptic electronics, which has motivated the emergence of optical-stimulated synapses, optical-assisted synapses, and optical-output synapses. Considering the energy consumption and operational mode, all-optical stimulated synapses are the preferred development direction for future AI compared with complex synergistic stimuli. Because of this, exploiting superior light absorption properties of MHPs for developing all-optical modulated optoelectronic synapses is urgently demanded to facilitate the advancement of neuromorphic devices.

(iii) Innovative applications. Until now, the majority of efforts are concentrated on simple simulations of synaptic behaviors, which remain in the initial stage, without a standardized model for evaluating synaptic devices. In terms of MHP materials, synaptic devices possessing a single function responding to optical stimuli alone have already failed to satisfy the demands of AI, and stretchable optoelectronic sensorimotor synapses based on MHPs by their inherently high mechanical flexibility deserve to be exploited as well. In addition, the evolution of these MHP-based optoelectronic synapses remains essential for the development of future neuromorphic systems, such as AIVs, wearable electronics, and human-machine interfaces.

Funding. National Key Research and Development Program of the Ministry of Science and Technology (2021YFA1200700, 2022YFB4400100); China National Funds for Distinguished Young Scientists (61925403); China National Funds for Outstanding Young Scientists (62122024); National Natural Science Foundation of China (12174094, 62134001, 62274060); Natural Science Foundation of Hunan Province (2021JJ20028, 2021RC5004); Guangdong Basic and Applied Basic Research Foundation-Regional Joint Fund (2020B1515120040); Shenzhen Science and Technology Research Funding (JCYJ2020shy0109115408041); Strategic Priority Research Program of Chinese Academy of Sciences (XDB30000000); Key Research and Development Program of Hunan Province of China (2022WK2001); Natural Science Foundation of Changsha (kq2004002).

Disclosures. The authors declare no conflicts of interests.

Data Availability. Data underlying the results presented in this paper are not publicly available at this time but may be obtained from the authors upon reasonable request.

REFERENCES

1. C.-M. Yang, T.-C. Chen, D. Verma, L.-J. Li, B. Liu, W.-H. Chang, and C.-S. Lai, "Bidirectional all-optical synapses based on a 2D Bi_2O_2Se/graphene hybrid structure for multifunctional optoelectronics," Adv. Funct. Mater. **30**, 2001598 (2020).
2. L. Zhou, S. Yang, G. Ding, J.-Q. Yang, Y. Ren, S.-R. Zhang, J.-Y. Mao, Y. Yang, Y. Zhou, and S.-T. Han, "Tunable synaptic behavior realized in C_3N composite based memristor," Nano Energy **58**, 293–303 (2019).
3. S.-R. Zhang, L. Zhou, J.-Y. Mao, Y. Ren, J.-Q. Yang, G.-H. Yang, X. Zhu, S.-T. Han, V. A. Roy, and Y. Zhou, "Artificial synapse emulated by charge trapping-based resistive switching device," Adv. Mater. Technol. **4**, 1800342 (2019).
4. X. Yan, J. Zhao, S. Liu, Z. Zhou, Q. Liu, J. Chen, and X. Y. Liu, "Memristor with Ag-cluster-doped TiO_2 films as artificial synapse for neuroinspired computing," Adv. Funct. Mater. **28**, 1705320 (2018).
5. F. A. Azevedo, L. R. Carvalho, L. T. Grinberg, J. M. Farfel, R. E. Ferretti, R. E. Leite, W. J. Filho, R. Lent, and S. Herculano-Houzel, "Equal numbers of neuronal and nonneuronal cells make the human brain an isometrically scaled-up primate brain," J. Comp. Neurol. **513**, 532–541 (2009).
6. D. R. Chialvo, "Emergent complex neural dynamics," Nat. Phys. **6**, 744–750 (2010).
7. Y. Tang, J. R. Nyengaard, D. M. De Groot, and H. J. G. Gundersen, "Total regional and global number of synapses in the human brain neocortex," Synapse **41**, 258–273 (2001).

8. Z. Zou, Y. Kim, F. Imani, H. Alimohamadi, R. Cammarota, and M. Imani, "Scalable edge-based hyperdimensional learning system with brain-like neural adaptation," in *Proceedings of the International Conference for High Performance Computing, Networking, Storage and Analysis* (2021), pp. 1–15.
9. R. Legenstein, "Nanoscale connections for brain-like circuits," Nature **521**, 37–38 (2015).
10. S. B. Eryilmaz, D. Kuzum, R. Jeyasingh, S. Kim, M. BrightSky, C. Lam, and H.-S. P. Wong, "Brain-like associative learning using a nanoscale non-volatile phase change synaptic device array," Front. Neurosci. **8**, 205 (2014).
11. M. V. DeBole, B. Taba, A. Amir, F. Akopyan, A. Andreopoulos, W. P. Risk, J. Kusnitz, C. O. Otero, T. K. Nayak, R. Appuswamy, P. J. Carlson, A. S. Cassidy, P. Datta, S. K. Esser, G. J. Garreau, K. L. Holland, S. Lekuch, M. Mastro, J. McKinstry, C. di Nolfo, B. Paulovicks, J. Sawada, K. Schleupen, B. G. Shaw, J. L. Klamo, M. D. Flickner, J. V. Arthur, and D. S. Modha, "TrueNorth: accelerating from zero to 64 million neurons in 10 years," Computer **52**, 20–29 (2019).
12. F. Akopyan, J. Sawada, A. Cassidy, R. Alvarez-Icaza, J. Arthur, P. Merolla, N. Imam, Y. Nakamura, P. Datta, G.-J. Nam, B. Taba, M. Beakes, B. Brezzo, J. B. Kuang, R. Manohar, W. P. Risk, B. Jackson, and D. S. Modha, "TrueNorth: design and tool flow of a 65 mW 1 million neuron programmable neurosynaptic chip," IEEE Trans. Comput. Aided Des. Integr. Circuits Syst. **34**, 1537–1557 (2015).
13. G. Haessig, A. Cassidy, R. Alvarez, R. Benosman, and G. Orchard, "Spiking optical flow for event-based sensors using IBM's TrueNorth neurosynaptic system," IEEE Trans. Biomed. Circuits Syst. **12**, 860–870 (2018).
14. S. Oh, Z. Huang, Y. Shi, and D. Kuzum, "The impact of resistance drift of phase change memory (PCM) synaptic devices on artificial neural network performance," IEEE Electron Device Lett. **40**, 1325–1328 (2019).
15. S. La Barbera, D. R. Ly, G. Navarro, N. Castellani, O. Cueto, G. Bourgeois, B. De Salvo, E. Nowak, D. Querlioz, and E. Vianello, "Narrow heater bottom electrode-based phase change memory as a bidirectional artificial synapse," Adv. Electron. Mater. **4**, 1800223 (2018).
16. S. Yu, Y. Wu, R. Jeyasingh, D. Kuzum, and H.-S. P. Wong, "An electronic synapse device based on metal oxide resistive switching memory for neuromorphic computation," IEEE Trans. Electron Devices **58**, 2729–2737 (2011).
17. X. Yan, Z. Zhou, B. Ding, J. Zhao, and Y. Zhang, "Superior resistive switching memory and biological synapse properties based on a simple TiN/SiO_2/p-Si tunneling junction structure," J. Mater. Chem. C **5**, 2259–2267 (2017).
18. M. Lederer, T. Kämpfe, T. Ali, F. Müller, R. Olivo, R. Hoffmann, N. Laleni, and K. Seidel, "Ferroelectric field effect transistors as a synapse for neuromorphic application," IEEE Trans. Electron Devices **68**, 2295–2300 (2021).
19. B. Jeong, P. Gkoupidenis, and K. Asadi, "Solution-processed perovskite field-effect transistor artificial synapses," Adv. Mater. **33**, 2104034 (2021).
20. W. Huang, P. Hang, Y. Wang, K. Wang, S. Han, Z. Chen, W. Peng, Y. Zhu, M. Xu, Y. Zhang, Y. Fang, X. Yu, D. Yang, and X. Pi, "Zero-power optoelectronic synaptic devices," Nano Energy **73**, 104790 (2020).
21. H. Duan, K. Javaid, L. Liang, L. Huang, J. Yu, H. Zhang, J. Gao, F. Zhuge, T.-C. Chang, and H. Cao, "Broadband optoelectronic synaptic thin-film transistors based on oxide semiconductors," Phys. Status Solidi RRL **14**, 1900630 (2020).
22. H. Li, X. Jiang, W. Ye, H. Zhang, L. Zhou, F. Zhang, D. She, Y. Zhou, and S.-T. Han, "Fully photon modulated heterostructure for neuromorphic computing," Nano Energy **65**, 104000 (2019).
23. L. Yin, W. Huang, R. Xiao, W. Peng, Y. Zhu, Y. Zhang, X. Pi, and D. Yang, "Optically stimulated synaptic devices based on the hybrid structure of silicon nanomembrane and perovskite," Nano Lett. **20**, 3378–3387 (2020).
24. Q. Li, T. Wang, Y. Fang, X. Hu, C. Tang, X. Wu, H. Zhu, L. Ji, Q.-Q. Sun, D. W. Zhang, and L. Chen, "Ultralow power wearable organic ferroelectric device for optoelectronic neuromorphic computing," Nano Lett. **22**, 6435–6443 (2022).
25. Y. Sun, M. Li, Y. Ding, H. Wang, H. Wang, Z. Chen, and D. Xie, "Programmable van-der-Waals heterostructure-enabled optoelectronic synaptic floating-gate transistors with ultra-low energy consumption," InfoMat **4**, e12317 (2022).
26. N. Li, C. He, Q. Wang, J. Tang, Q. Zhang, C. Shen, J. Tang, H. Huang, S. Wang, J. Li, B. Huang, Z. Wei, Y. Guo, J. Yuan, W. Yang, R. Yang, D. Shi, and G. Zhang, "Gate-tunable large-scale flexible monolayer MoS_2 devices for photodetectors and optoelectronic synapses," Nano Res. **15**, 5418–5424 (2022).
27. R. Zhu, H. Liang, S. Hu, Y. Wang, and Z. Mei, "Amorphous-Ga_2O_3 optoelectronic synapses with ultra-low energy consumption," Adv. Electron. Mater. **8**, 2100741 (2022).
28. P. Lei, H. Duan, L. Qin, X. Wei, R. Tao, Z. Wang, F. Guo, M. Song, W. Jie, and J. Hao, "High-performance memristor based on 2D layered BiOI nanosheet for low-power artificial optoelectronic synapses," Adv. Funct. Mater. **32**, 2201276 (2022).
29. W. Zhang, G. E. Eperon, and H. J. Snaith, "Metal halide perovskites for energy applications," Nat. Energy **1**, 16048 (2016).
30. C. Zhou, H. Lin, Q. He, L. Xu, M. Worku, M. Chaaban, S. Lee, X. Shi, M.-H. Du, and B. Ma, "Low dimensional metal halide perovskites and hybrids," Mater. Sci. Eng. R **137**, 38–65 (2019).
31. M. Baranowski and P. Plochocka, "Excitons in metal-halide perovskites," Adv. Energy Mater. **10**, 1903659 (2020).
32. S. D. Stranks and H. J. Snaith, "Metal-halide perovskites for photovoltaic and light-emitting devices," Nat. Nanotechnol. **10**, 391–402 (2015).
33. X.-K. Liu, W. Xu, S. Bai, Y. Jin, J. Wang, R. H. Friend, and F. Gao, "Metal halide perovskites for light-emitting diodes," Nat. Mater. **20**, 10–21 (2021).
34. L. Lei, Q. Dong, K. Gundogdu, and F. So, "Metal halide perovskites for laser applications," Adv. Funct. Mater. **31**, 2010144 (2021).
35. Y. Hou, L. Wang, X. Zou, D. Wan, C. Liu, G. Li, X. Liu, Y. Liu, C. Jiang, J. C. Ho, and L. Liao, "Substantially improving device performance of all-inorganic perovskite-based phototransistors via indium tin oxide nanowire incorporation," Small **16**, 1905609 (2020).
36. S. Wei, F. Wang, X. Zou, L. Wang, C. Liu, X. Liu, W. Hu, Z. Fan, J. C. Ho, and L. Liao, "Flexible quasi-2D perovskite/IGZO phototransistors for ultrasensitive and broadband photodetection," Adv. Mater. **32**, 1907527 (2020).
37. L. Wang, X. Zou, J. Lin, J. Jiang, Y. Liu, X. Liu, X. Zhao, Y. F. Liu, J. C. Ho, and L. Liao, "Perovskite/black phosphorus/MoS_2 photogate reversed photodiodes with ultrahigh light on/off ratio and fast response," ACS Nano **13**, 4804–4813 (2019).
38. J. Jiang, X. Zou, Y. Lv, Y. Liu, W. Xu, Q. Tao, Y. Chai, and L. Liao, "Rational design of Al_2O_3/2D perovskite heterostructure dielectric for high performance MoS_2 phototransistors," Nat. Commun. **11**, 4266 (2020).
39. Q. Tian, R. Hong, C. Liu, X. Hong, S. Zhang, L. Wang, Y. Lv, X. Liu, X. Zou, and L. Liao, "Flexible SnO optoelectronic memory based on light-dependent ionic migration in Ruddlesden–Popper perovskite," Nano Lett. **22**, 494–500 (2021).
40. B. R. Sutherland and E. H. Sargent, "Perovskite photonic sources," Nat. Photonics **10**, 295–302 (2016).
41. H. Dong, C. Zhang, X. Liu, J. Yao, and Y. S. Zhao, "Materials chemistry and engineering in metal halide perovskite lasers," Chem. Soc. Rev. **49**, 951–982 (2020).
42. F. P. Garca de Arquer, A. Armin, P. Meredith, and E. H. Sargent, "Solution-processed semiconductors for next-generation photodetectors," Nat. Rev. Mater. **2**, 16100 (2017).
43. Z.-K. Tan, R. S. Moghaddam, M. L. Lai, P. Docampo, R. Higler, F. Deschler, M. Price, A. Sadhanala, L. M. Pazos, D. Credgington, F. Hanusch, T. Bein, H. J. Snaith, and R. H. Friend, "Bright light-emitting diodes based on organometal halide perovskite," Nat. Nanotechnol. **9**, 687–692 (2014).
44. L. M. Herz, "Charge-carrier mobilities in metal halide perovskites: fundamental mechanisms and limits," ACS Energy Lett. **2**, 1539–1548 (2017).
45. G. Zhou, B. Su, J. Huang, Q. Zhang, and Z. Xia, "Broad-band emission in metal halide perovskites: Mechanism, materials, and applications," Mater. Sci. Eng. R **141**, 100548 (2020).

46. H.-S. Kim, I. Mora-Sero, V. Gonzalez-Pedro, F. Fabregat-Santiago, E. J. Juarez-Perez, N.-G. Park, and J. Bisquert, "Mechanism of carrier accumulation in perovskite thin-absorber solar cells," Nat. Commun. **4**, 2242 (2013).
47. J. M. Frost, K. T. Butler, F. Brivio, C. H. Hendon, M. Van Schilfgaarde, and A. Walsh, "Atomistic origins of high-performance in hybrid halide perovskite solar cells," Nano Lett. **14**, 2584–2590 (2014).
48. H. J. Snaith, A. Abate, J. M. Ball, G. E. Eperon, T. Leijtens, N. K. Noel, S. D. Stranks, J. T.-W. Wang, K. Wojciechowski, and W. Zhang, "Anomalous hysteresis in perovskite solar cells," J. Phys. Chem. Lett. **5**, 1511–1515 (2014).
49. Y. Zhang, M. Liu, G. E. Eperon, T. C. Leijtens, D. McMeekin, M. Saliba, W. Zhang, M. de Bastiani, A. Petrozza, L. M. Herz, M. B. Johnston, H. Lin, and H. J. Snaith, "Charge selective contacts, mobile ions and anomalous hysteresis in organic–inorganic perovskite solar cells," Mater. Horiz. **2**, 315–322 (2015).
50. D. A. Jacobs, Y. Wu, H. Shen, C. Barugkin, F. J. Beck, T. P. White, K. Weber, and K. R. Catchpole, "Hysteresis phenomena in perovskite solar cells: the many and varied effects of ionic accumulation," Phys. Chem. Chem. Phys. **19**, 3094–3103 (2017).
51. J. Lao, M. Yan, B. Tian, C. Jiang, C. Luo, Z. Xie, Q. Zhu, Z. Bao, N. Zhong, X. Tang, L. Sun, G. Wu, J. Wang, H. Peng, J. Chu, and C. Duan, "Ultralow-power machine vision with self-powered sensor reservoir," Adv. Sci. Weinheim **9**, 2106092 (2022).
52. Y. Song, X. Xu, Y. Zhang, Z. Han, J. Liu, J. Li, and Y. Zou, "Light-induced perovskite dynamic transformation enabling a photodetector to mimic a neuromorphic vision sensing system," J. Mater. Chem. C **10**, 3387–3395 (2022).
53. J. Gong, H. Wei, Y. Ni, S. Zhang, Y. Du, and W. Xu, "Methylammonium halide-doped perovskite artificial synapse for light-assisted environmental perception and learning," Mater. Today Phys. **21**, 100540 (2021).
54. S. Hu, Y. Liu, T. Chen, Z. Liu, Q. Yu, L. Deng, Y. Yin, and S. Hosaka, "Emulating the paired-pulse facilitation of a biological synapse with a NiO_x-based memristor," Appl. Phys. Lett. **102**, 183510 (2013).
55. Y. Wang, Y. Zhu, Y. Li, Y. Zhang, D. Yang, and X. Pi, "Dual-modal optoelectronic synaptic devices with versatile synaptic plasticity," Adv. Funct. Mater. **32**, 2107973 (2022).
56. J. Zhang, T. Sun, S. Zeng, D. Hao, B. Yang, S. Dai, D. Liu, L. Xiong, C. Zhao, and J. Huang, "Tailoring neuroplasticity in flexible perovskite QDS-based optoelectronic synaptic transistors by dual modes modulation," Nano Energy **95**, 106987 (2022).
57. C. Han, X. Han, J. Han, M. He, S. Peng, C. Zhang, X. Liu, J. Gou, and J. Wang, "Light-stimulated synaptic transistor with high PPF feature for artificial visual perception system application," Adv. Funct. Mater. **32**, 2113053 (2022).
58. Y. Cheng, H. Li, B. Liu, L. Jiang, M. Liu, H. Huang, J. Yang, J. He, and J. Jiang, "Vertical 0D-perovskite/2D-MoS_2 van der Waals heterojunction phototransistor for emulating photoelectric-synergistically classical Pavlovian conditioning and neural coding dynamics," Small **16**, 2005217 (2020).
59. T.-J. Lee, K.-R. Yun, S.-K. Kim, J.-H. Kim, J. Jin, K.-B. Sim, D.-H. Lee, G. W. Hwang, and T.-Y. Seong, "Realization of an artificial visual nervous system using an integrated optoelectronic device array," Adv. Mater. **33**, 2105485 (2021).
60. X. Huang, Q. Li, W. Shi, K. Liu, Y. Zhang, Y. Liu, X. Wei, Z. Zhao, Y. Guo, and Y. Liu, "Dual-mode learning of ambipolar synaptic phototransistor based on 2D perovskite/organic heterojunction for flexible color recognizable visual system," Small **17**, 2102820 (2021).
61. Y. Wang, Z. Lv, J. Chen, Z. Wang, Y. Zhou, L. Zhou, X. Chen, and S.-T. Han, "Photonic synapses based on inorganic perovskite quantum dots for neuromorphic computing," Adv. Mater. **30**, 1802883 (2018).
62. J. Liu, Z. Yang, Z. Gong, Z. Shen, Y. Ye, B. Yang, Y. Qiu, B. Ye, L. Xu, T. Guo, and S. Xu, "Weak light-stimulated synaptic hybrid phototransistors based on island like perovskite films prepared by spin coating," ACS Appl. Mater. Interfaces **13**, 13362–13371 (2021).
63. L. Yin, C. Han, Q. Zhang, Z. Ni, S. Zhao, K. Wang, D. Li, M. Xu, H. Wu, X. Pi, and D. Yang, "Synaptic silicon-nanocrystal phototransistors for neuromorphic computing," Nano Energy **63**, 103859 (2019).
64. Z. Xiao and J. Huang, "Energy-efficient hybrid perovskite memristors and synaptic devices," Adv. Electron. Mater. **2**, 1600100 (2016).
65. T.-Y. Wang, J.-L. Meng, M.-Y. Rao, Z.-Y. He, L. Chen, H. Zhu, Q.-Q. Sun, S.-J. Ding, W.-Z. Bao, P. Zhou, and D. W. Zhang, "Three-dimensional nanoscale flexible memristor networks with ultralow power for information transmission and processing application," Nano Lett. **20**, 4111–4120 (2020).
66. J. Li, C. Ge, J. Du, C. Wang, G. Yang, and K. Jin, "Reproducible ultrathin ferroelectric domain switching for high-performance neuromorphic computing," Adv. Mater. **32**, 1905764 (2020).
67. X. Hong, Y. Huang, Q. Tian, S. Zhang, C. Liu, L. Wang, K. Zhang, J. Sun, L. Liao, and X. Zou, "Two-dimensional perovskite-gated AlGaN/GaN high-electron-mobility-transistor for neuromorphic vision sensor," Adv. Sci. Weinheim **9**, 2202019 (2022).
68. E. S. Fortune and G. J. Rose, "Short-term synaptic plasticity as a temporal filter," Trends Neurosci. **24**, 381–385 (2001).
69. L. Q. Zhu, C. J. Wan, L. Q. Guo, Y. Shi, and Q. Wan, "Artificial synapse network on inorganic proton conductor for neuromorphic systems," Nat. Commun. **5**, 3158 (2014).
70. D. O. Hebb, *The Organization of Behavior: A Neuropsychological Theory* (Psychology, 2005).
71. G.-Q. Bi and M.-M. Poo, "Synaptic modifications in cultured hippocampal neurons: dependence on spike timing, synaptic strength, and postsynaptic cell type," J. Neurosci. **18**, 10464–10472 (1998).
72. R. S. Zucker and W. G. Regehr, "Short-term synaptic plasticity," Annu. Rev. Physiol. **64**, 355–405 (2002).
73. S. Martin, P. D. Grimwood, and R. G. Morris, "Synaptic plasticity and memory: an evaluation of the hypothesis," Annu. Rev. Neurosci. **23**, 649–711 (2000).
74. P. P. Atluri and W. G. Regehr, "Determinants of the time course of facilitation at the granule cell to Purkinje cell synapse," J. Neurosci. **16**, 5661–5671 (1996).
75. Y.-X. Hou, Y. Li, Z.-C. Zhang, J.-Q. Li, D.-H. Qi, X.-D. Chen, J.-J. Wang, B.-W. Yao, M.-X. Yu, T.-B. Lu, and J. Zhang, "Large-scale and flexible optical synapses for neuromorphic computing and integrated visible information sensing memory processing," ACS Nano **15**, 1497–1508 (2020).
76. X. Zhu and W. D. Lu, "Optogenetics-inspired tunable synaptic functions in memristors," ACS Nano **12**, 1242–1249 (2018).
77. B. Sturman, E. Podivilov, and M. Gorkunov, "Origin of stretched exponential relaxation for hopping-transport models," Phys. Rev. Lett. **91**, 176602 (2003).
78. J. Kakalios and R. Street, and N. W. Jackson, "Stretched-exponential relaxation arising from dispersive diffusion of hydrogen in amorphous silicon," Phys. Rev. Lett. **59**, 1037–1040 (1987).
79. J. Phillips, "Stretched exponential relaxation in molecular and electronic glasses," Rep. Prog. Phys. **59**, 1133–1207 (1996).
80. S. Gao, G. Liu, H. Yang, C. Hu, Q. Chen, G. Gong, W. Xue, X. Yi, J. Shang, and R.-W. Li, "An oxide Schottky junction artificial optoelectronic synapse," ACS Nano **13**, 2634–2642 (2019).
81. S. Wang, C. Chen, Z. Yu, Y. He, X. Chen, Q. Wan, Y. Shi, D. W. Zhang, H. Zhou, X. Wang, and P. Zhou, "A MoS_2/PTCDA hybrid heterojunction synapse with efficient photoelectric dual modulation and versatility," Adv. Mater. **31**, 1806227 (2019).
82. Y. Wang, J. Yang, Z. Wang, J. Chen, Q. Yang, Z. Lv, Y. Zhou, Y. Zhai, Z. Li, and S.-T. Han, "Near-infrared annihilation of conductive filaments in quasiplane $MoSe_2$/Bi_2Se_3 nanosheets for mimicking heterosynaptic plasticity," Small **15**, 1805431 (2019).
83. D. Debanne, N. C. Guerineau, B. Gähwiler, and S. M. Thompson, "Paired-pulse facilitation and depression at unitary synapses in rat hippocampus: quantal fluctuation affects subsequent release," J. Physiol. **491**, 163–176 (1996).
84. Y. H. Liu, L. Q. Zhu, P. Feng, Y. Shi, and Q. Wan, "Freestanding artificial synapses based on laterally proton-coupled transistors on chitosan membranes," Adv. Mater. **27**, 5599–5604 (2015).
85. G. Liu, C. Wang, W. Zhang, L. Pan, C. Zhang, X. Yang, F. Fan, Y. Chen, and R.-W. Li, "Organic biomimicking memristor for information storage and processing applications," Adv. Electron. Mater. **2**, 1500298 (2016).
86. J.-T. Yang, C. Ge, J.-Y. Du, H.-Y. Huang, M. He, C. Wang, H.-B. Lu, G.-Z. Yang, and K.-J. Jin, "Artificial synapses emulated by an

electrolyte-gated tungsten-oxide transistor," Adv. Mater. **30**, 1801548 (2018).
87. F. Huang, F. Fang, Y. Zheng, Q. You, H. Li, S. Fang, X. Cong, K. Jiang, Y. Wang, C. Han, W. Chen, and Y. Shi, "Visible-light stimulated synaptic plasticity in amorphous indium-gallium-zinc oxide enabled by monocrystalline double perovskite for high-performance neuromorphic applications," Nano Res. **16**, 1304–1312 (2022).
88. Y. Li, Y. Zhong, L. Xu, J. Zhang, X. Xu, H. Sun, and X. Miao, "Ultrafast synaptic events in a chalcogenide memristor," Sci. Rep. **3**, 1619 (2013).
89. R. C. Atkinson and R. M. Shiffrin, "Human memory: a proposed system and its control processes," in *Psychology of Learning and Motivation* (Elsevier, 1968), Vol. **2**, pp. 89–195.
90. S. Zhang, L. Yang, C. Jiang, L. Sun, K. Guo, H. Han, and W. Xu, "Digitally aligned ZnO nanowire array based synaptic transistors with intrinsically controlled plasticity for short-term computation and long-term memory," Nanoscale **13**, 19190–19199 (2021).
91. M.-K. Kim and J.-S. Lee, "Short-term plasticity and long-term potentiation in artificial biosynapses with diffusive dynamics," ACS Nano **12**, 1680–1687 (2018).
92. A. Suvrathan, H. L. Payne, and J. L. Raymond, "Timing rules for synaptic plasticity matched to behavioral function," Neuron **92**, 959–967 (2016).
93. G. Rachmuth, H. Z. Shouval, M. F. Bear, and C.-S. Poon, "A biophysically-based neuromorphic model of spike rate- and timing-dependent plasticity," Proc. Natl. Acad. Sci. USA **108**, E1266–E1274 (2011).
94. N. Andersen, N. Krauth, and S. Nabavi, "Hebbian plasticity *in vivo*: relevance and induction," Curr. Opin. Neurobiol. **45**, 188–192 (2017).
95. D. Fernandes and A. L. Carvalho, "Mechanisms of homeostatic plasticity in the excitatory synapse," J. Neurochem. **139**, 973–996 (2016).
96. K. Wang, S. Dai, Y. Zhao, Y. Wang, C. Liu, and J. Huang, "Light-stimulated synaptic transistors fabricated by a facile solution process based on inorganic perovskite quantum dots and organic semiconductors," Small **15**, 1900010 (2019).
97. E. Ercan, Y.-C. Lin, W.-C. Yang, and W.-C. Chen, "Self-assembled nanostructures of quantum dot/conjugated polymer hybrids for photonic synaptic transistors with ultralow energy consumption and zero-gate bias," Adv. Funct. Mater. **32**, 2107925 (2022).
98. M.-K. Song, H. Lee, J. H. Yoon, Y.-W. Song, S. D. Namgung, T. Sung, Y.-S. Lee, J.-S. Lee, K. T. Nam, and J.-Y. Kwon, "Humidity-induced synaptic plasticity of ZnO artificial synapses using peptide insulator for neuromorphic computing," J. Mater. Sci. Technol. **119**, 150–155 (2022).
99. M. H. Hennig, "Theoretical models of synaptic short term plasticity," Front. Comput. Neurosci. **7**, 45 (2013).
100. L. G. Morris and S. L. Hooper, "Muscle response to changing neuronal input in the lobster (*Panulirus interruptus*) stomatogastric system: spike number-versus spike frequency-dependent domains," J. Neurosci. **17**, 5956–5971 (1997).
101. P. Subin, A. Asha, K. Saji, and M. Jayaraj, "Spike-dependent plasticity modulation in TiO_2-based synaptic device," J. Mater. Sci. Mater. Electron. **32**, 13051–13061 (2021).
102. S. Poddar, Z. Chen, Z. Ma, Y. Zhang, C. L. J. Chan, B. Ren, Q. Zhang, D. Zhang, G. Shen, H. Zeng, and Z. Fan, "Robust lead-free perovskite nanowire array-based artificial synapses exemplifying gestalt principle of closure via a letter recognition scheme," Adv. Intell. Syst. **4**, 2200065 (2022).
103. S. Zhang, K. Guo, H. Han, H. Yu, H. Wei, J. Gong, and W. Xu, "Multiplexed neurotransmission emulated by a p–n cross nanowire synaptic transistor for satiety, depression, and drug withdrawal," Adv. Funct. Mater. **31**, 2101917 (2021).
104. J. Ren, H. Shen, Z. Liu, M. Xu, and D. Li, "Artificial synapses based on WSe_2 homojunction via vacancy migration," ACS Appl. Mater. Interfaces **14**, 21141–21149 (2022).
105. J. Gong, H. Yu, H. Wei, Y. Zheng, C. Yuan, M. Ma, H. Han, K. Guo, J. Xu, and W. Xu, "An air-stable two-dimensional perovskite artificial synapse," Semicond. Sci. Technol. **35**, 104001 (2020).
106. M. F. Bear and R. C. Malenka, "Synaptic plasticity: LTP and LTD," Curr. Opin. Neurobiol. **4**, 389–399 (1994).
107. T. Masquelier, R. Guyonneau, and S. J. Thorpe, "Spike timing dependent plasticity finds the start of repeating patterns in continuous spike trains," PLoS ONE **3**, e1377 (2008).
108. T. Masquelier, R. Guyonneau, and S. J. Thorpe, "Competitive STDP-based spike pattern learning," Neural Comput. **21**, 1259–1276 (2009).
109. L. A. Finelli, S. Haney, M. Bazhenov, M. Stopfer, and T. J. Sejnowski, "Synaptic learning rules and sparse coding in a model sensory system," PLoS Comput. Biol. **4**, e1000062 (2008).
110. D. O. Hebb, *The Organization of Behavior: A Neuropsychological Theory* (Wiley, 1949).
111. Y. Dan and M.-M. Poo, "Spike timing-dependent plasticity of neural circuits," Neuron **44**, 23–30 (2004).
112. P. C. Harikesh, C.-Y. Yang, D. Tu, J. Y. Gerasimov, A. M. Dar, A. Armada-Moreira, M. Massetti, R. Kroon, D. Bliman, R. Olsson, E. Stavrinidou, M. Berggren, and S. Fabiano, "Organic electrochemical neurons and synapses with ion mediated spiking," Nat. Commun. **13**, 1138 (2022).
113. J. Zhang and Z. Kourtzi, "Learning-dependent plasticity with and without training in the human brain," Proc. Natl. Acad. Sci. USA **107**, 13503–13508 (2010).
114. S. Song, K. D. Miller, and L. F. Abbott, "Competitive Hebbian learning through spike-timing-dependent synaptic plasticity," Nat. Neurosci. **3**, 919–926 (2000).
115. R. C. Froemke and Y. Dan, "Spike-timing-dependent synaptic modification induced by natural spike trains," Nature **416**, 433–438 (2002).
116. D. Kuzum, S. Yu, and H. P. Wong, "Synaptic electronics: materials, devices and applications," Nanotechnology **24**, 382001 (2013).
117. W. Xu, T. L. Nguyen, Y.-T. Kim, C. Wolf, R. Pfattner, J. Lopez, B.-G. Chae, S.-I. Kim, M. Y. Lee, E.-Y. Shin, Y.-Y. Noh, J. H. Oh, H. Hwang, C.-G. Park, H. Y. Woo, and T.-W. Lee, "Ultrasensitive artificial synapse based on conjugated polyelectrolyte," Nano Energy **48**, 575–581 (2018).
118. H. Tan, Z. Ni, W. Peng, S. Du, X. Liu, S. Zhao, W. Li, Z. Ye, M. Xu, Y. Xu, X. Pi, and D. Yang, "Broadband optoelectronic synaptic devices based on silicon nanocrystals for neuromorphic computing," Nano Energy **52**, 422–430 (2018).
119. P. Lennie, "The cost of cortical computation," Curr. Biol. **13**, 493–497 (2003).
120. I.-T. Wang, Y.-C. Lin, Y.-F. Wang, C.-W. Hsu, and T.-H. Hou, "3D synaptic architecture with ultralow sub-10 FJ energy per spike for neuromorphic computation," in *IEEE International Electron Devices Meeting* (IEEE, 2014), pp. 28.5.1–28.5.4.
121. M. Lee, W. Lee, S. Choi, J.-W. Jo, J. Kim, S. K. Park, and Y.-H. Kim, "Brain-inspired photonic neuromorphic devices using photodynamic amorphous oxide semiconductors and their persistent photoconductivity," Adv. Mater. **29**, 1700951 (2017).
122. H. Li, T. Chen, P. Liu, S. Hu, Y. Liu, Q. Zhang, and P. Lee, "A light-stimulated synaptic transistor with synaptic plasticity and memory functions based on $InGaZnO_x$–Al_2O_3 thin film structure," J. Appl. Phys. **119**, 244505 (2016).
123. S. Choi, S. Jang, J.-H. Moon, J. C. Kim, H. Y. Jeong, P. Jang, K.-J. Lee, and G. Wang, "A self-rectifying TaO_y/nanoporous TaO_x memristor synaptic array for learning and energy-efficient neuromorphic systems," NPG Asia Mater. **10**, 1097–1106 (2018).
124. T. Fu, X. Liu, H. Gao, J. E. Ward, X. Liu, B. Yin, Z. Wang, Y. Zhuo, D. J. Walker, J. Joshua Yang, J. Chen, D. R. Lovley, and J. Yao, "Bioinspired bio-voltage memristors," Nat. Commun. **11**, 13 (2020).
125. X. Feng, Y. Li, L. Wang, S. Chen, Z. G. Yu, W. C. Tan, N. Macadam, G. Hu, L. Huang, L. Chen, X. Gong, D. Chi, T. Hasan, A. V.-Y. Thean, Y.-W. Zhang, and K.-W. Ang, "A fully printed flexible MoS_2 memristive artificial synapse with femtojoule switching energy," Adv. Electron. Mater. **5**, 1900740 (2019).
126. F. Ma, Y. Zhu, Z. Xu, Y. Liu, X. Zheng, S. Ju, Q. Li, Z. Ni, H. Hu, Y. Chai, C. Wu, T. W. Kim, and F. Li, "Optoelectronic perovskite synapses for neuromorphic computing," Adv. Funct. Mater. **30**, 1908901 (2020).
127. Z. Xin, Y. Tan, T. Chen, E. Iranmanesh, L. Li, K.-C. Chang, S. Zhang, C. Liu, and H. Zhou, "Visible-light-stimulated synaptic InGaZnO

phototransistors enabled by wavelength-tunable perovskite quantum dots," Nano. Adv. **3**, 5046–5052 (2021).
128. Y. Park, M.-K. Kim, and J.-S. Lee, "2D layered metal-halide perovskite/oxide semiconductor-based broadband optoelectronic synaptic transistors with long-term visual memory," J. Mater. Chem. C **9**, 1429–1436 (2021).
129. K. Lee, H. Han, Y. Kim, J. Park, S. Jang, H. Lee, S. W. Lee, H. Kim, Y. Kim, T. Kim, D. Kim, G. Wang, and C. Park, "Retina-inspired structurally tunable synaptic perovskite nanocones," Adv. Funct. Mater. **31**, 2105596 (2021).
130. J. Lao, W. Xu, C. Jiang, N. Zhong, B. Tian, H. Lin, C. Luo, J. Travas-Sejdic, H. Peng, and C.-G. Duan, "Artificial synapse based on organic–inorganic hybrid perovskite with electric and optical modulation," Adv. Electron. Mater. **7**, 2100291 (2021).
131. H. Duan, L. Liang, Z. Wu, H. Zhang, L. Huang, and H. Cao, "IGZO/$CsPbBr_3$-nanoparticles/IGZO neuromorphic phototransistors and their optoelectronic coupling applications," ACS Appl. Mater. Interfaces **13**, 30165–30173 (2021).
132. Y. Cao, X. Sha, X. Bai, Y. Shao, Y. Gao, Y.-M. Wei, L. Meng, N. Zhou, J. Liu, B. Li, X.-F. Yu, and J. Li, "Ultralow light-power consuming photonic synapses based on ultrasensitive perovskite/indium-gallium-zinc-oxide heterojunction phototransistors," Adv. Electron. Mater. **8**, 2100902 (2022).
133. X. Yang, Z. Xiong, Y. Chen, Y. Ren, L. Zhou, H. Li, Y. Zhou, F. Pan, and S.-T. Han, "A self-powered artificial retina perception system for image preprocessing based on photovoltaic devices and memristive arrays," Nano Energy **78**, 105246 (2020).
134. Y. Sun, L. Qian, D. Xie, Y. Lin, M. Sun, W. Li, L. Ding, T. Ren, and T. Palacios, "Photoelectric synaptic plasticity realized by 2D perovskite," Adv. Funct. Mater. **29**, 1902538 (2019).
135. Z. Liu, S. Dai, Y. Wang, B. Yang, D. Hao, D. Liu, Y. Zhao, L. Fang, Q. Ou, S. Jin, J. Zhao, and J. Huang, "Photoresponsive transistors based on lead-free perovskite and carbon nanotubes," Adv. Funct. Mater. **30**, 1906335 (2020).
136. W. He, Y. Fang, H. Yang, X. Wu, L. He, H. Chen, and T. Guo, "A multi-input light-stimulated synaptic transistor for complex neuromorphic computing," J. Mater. Chem. C **7**, 12523–12531 (2019).
137. L. Qian, Y. Sun, M. Wu, C. Li, D. Xie, L. Ding, and G. Shi, "A lead-free two-dimensional perovskite for a high-performance flexible photoconductor and a light-stimulated synaptic device," Nanoscale **10**, 6837–6843 (2018).
138. B. Pradhan, S. Das, J. Li, F. Chowdhury, J. Cherusseri, D. Pandey, D. Dev, A. Krishnaprasad, E. Barrios, A. Towers, A. Gesquiere, L. Tetard, T. Roy, and J. Thomas, "Ultrasensitive and ultrathin phototransistors and photonic synapses using perovskite quantum dots grown from graphene lattice," Sci. Adv. **6**, eaay5225 (2020).
139. L. Yang, M. Singh, S.-W. Shen, K.-Y. Chih, S.-W. Liu, C.-I. Wu, C.-W. Chu, and H.-W. Lin, "Transparent and flexible inorganic perovskite photonic artificial synapses with dual-mode operation," Adv. Funct. Mater. **31**, 2008259 (2021).
140. L. Chua, "Memristor-the missing circuit element," IEEE Trans. Circuit Theory **18**, 507–519 (1971).
141. R. A. John, Y. Demirağ, Y. Shynkarenko, Y. Berezovska, N. Ohannessian, M. Payvand, P. Zeng, M. I. Bodnarchuk, F. Krumeich, G. Kara, I. Shorubalko, M. V. Nair, G. A. Cooke, T. Lippert, G. Indiveri, and M. V. Kovalenko, "Reconfigurable halide perovskite nanocrystal memristors for neuromorphic computing," Nat. Commun. **13**, 2074 (2022).
142. C. Wang, G.-Q. Mao, M. Huang, E. Huang, Z. Zhang, J. Yuan, W. Cheng, K.-H. Xue, X. Wang, and X. Miao, "HfO_x/AlO_y superlattice-like memristive synapse," Adv. Sci. Weinheim **9**, 2201446 (2022).
143. A. Wedig, M. Luebben, D.-Y. Cho, M. Moors, K. Skaja, V. Rana, T. Hasegawa, K. K. Adepalli, B. Yildiz, R. Waser, and I. Valov, "Nanoscale cation motion in TaO_x, HfO_x and TiO_x memristive systems," Nat. Nanotechnol. **11**, 67–74 (2016).
144. M. D. Pickett, G. Medeiros-Ribeiro, and R. S. Williams, "A scalable neuristor built with Mott memristors," Nat. Mater. **12**, 114–117 (2013).
145. K. Wen, Y. Fan, G. Wang, L. Jin, X. Li, Z. Li, Y. Zhang, and B. Xiong, "Aging behavior and precipitate characterization of a high Zn-containing Al-Zn-Mg-Cu alloy with various tempers," Mater. Des. **101**, 16–23 (2016).
146. J. Du, D. Xie, Q. Zhang, H. Zhong, F. Meng, X. Fu, Q. Sun, H. Ni, T. Li, E.-J. Guo, H. Guo, M. He, C. Wang, L. Gu, X. Xu, G. Zhang, G. Yang, K. Jin, and C. Ge, "A robust neuromorphic vision sensor with optical control of ferroelectric switching," Nano Energy **89**, 106439 (2021).
147. S. Lan, X. Wang, R. Yu, C. Zhou, M. Wang, and X. Cai, "Organic synaptic transistors based on a hybrid trapping layer for neuromorphic computing," IEEE Electron Device Lett. **43**, 1255–1258 (2022).
148. G. Feng, J. Jiang, Y. Li, D. Xie, B. Tian, and Q. Wan, "Flexible vertical photogating transistor network with an ultrashort channel for in-sensor visual nociceptor," Adv. Funct. Mater. **31**, 2104327 (2021).
149. K. Wang, J. Chen, and X. Yan, "MXene Ti_3C_2 memristor for neuromorphic behavior and decimal arithmetic operation applications," Nano Energy **79**, 105453 (2021).
150. Y. Ren, W.-C. Lin, L.-Y. Ting, G. Ding, B. Yang, J.-Q. Yang, H.-H. Chou, S.-T. Han, and Y. Zhou, "Iridium-based polymer for memristive devices with integrated logic and arithmetic applications," J. Mater. Chem. C **8**, 16845–16857 (2020).
151. J. Feldmann, M. Stegmaier, N. Gruhler, C. Ríos, H. Bhaskaran, C. Wright, and W. Pernice, "Calculating with light using a chip-scale all-optical abacus," Nat. Commun. **8**, 1256 (2017).
152. C. D. Wright, P. Hosseini, and J. A. V. Diosdado, "Beyond von-Neumann computing with nanoscale phase-change memory devices," Adv. Funct. Mater. **23**, 2248–2254 (2013).
153. J. Wang, J. Wang, J. Zhang, W. Huang, X. Wang, and M. Zhang, "Ultralow-power synaptic transistors based on Ta_2O_5/Al_2O_3 bilayer dielectric for algebraic arithmetic," Adv. Electron. Mater. **8**, 2100922 (2022).
154. Y. Li, R. Ji, P. Zhao, J. Lao, C. Jiang, B. Tian, C. Luo, H. Lin, H. Peng, and C.-G. Duan, "Transparent optoelectronic synapse based on a cui electrode for arithmetic operation," ACS Appl. Electron. Mater. **4**, 1989–1996 (2022).
155. C. D. Wright, Y. Liu, K. I. Kohary, M. M. Aziz, and R. J. Hicken, "Arithmetic and biologically-inspired computing using phase-change materials," Adv. Mater. **23**, 3408–3413 (2011).
156. W. Hu, J. Jiang, D. Xie, B. Liu, J. Yang, and J. He, "Proton–electron-coupled MoS_2 synaptic transistors with a natural renewable biopolymer neurotransmitter for brain-inspired neuromorphic learning," J. Mater. Chem. C **7**, 682–691 (2019).
157. S. Zhao, Z. Ni, H. Tan, Y. Wang, H. Jin, T. Nie, M. Xu, X. Pi, and D. Yang, "Electroluminescent synaptic devices with logic functions," Nano Energy **54**, 383–389 (2018).
158. D. Hao, J. Zhang, S. Dai, J. Zhang, and J. Huang, "Perovskite/organic semiconductor-based photonic synaptic transistor for artificial visual system," ACS Appl. Mater. Interfaces **12**, 39487–39495 (2020).
159. Y. Wang, Y. Zheng, J. Gao, T. Jin, E. Li, X. Lian, X. Pan, C. Han, H. Chen, and W. Chen, "Band-tailored van der Waals heterostructure for multilevel memory and artificial synapse," InfoMat **3**, 917–928 (2021).
160. J. Yu, X. Yang, G. Gao, Y. Xiong, Y. Wang, J. Han, Y. Chen, H. Zhang, Q. Sun, and Z. L. Wang, "Bioinspired mechano-photonic artificial synapse based on graphene/MoS_2 heterostructure," Sci. Adv. **7**, eabd9117 (2021).
161. G. Pedretti, V. Milo, S. Ambrogio, R. Carboni, S. Bianchi, A. Calderoni, N. Ramaswamy, A. Spinelli, and D. Ielmini, "Memristive neural network for on-line learning and tracking with brain-inspired spike timing dependent plasticity," Sci. Rep. **7**, 5288 (2017).
162. Z. Yang and A. F. Murray, "An artificial early visual model adopting spike-timing-dependent plasticity," Neurocomputing **69**, 1904–1911 (2006).
163. A. Oliveri, R. Rizzo, and A. Chella, "An application of spike-timing-dependent plasticity to readout circuit for liquid state machine," in *International Joint Conference on Neural Networks* (IEEE, 2007), pp. 1441–1445.
164. T. J. Koickal, L. C. Gouveia, and A. Hamilton, "A programmable spike-timing based circuit block for reconfigurable neuromorphic computing," Neurocomputing **72**, 3609–3616 (2009).

165. N. Raeis-Hosseini, Y. Park, and J.-S. Lee, "Flexible artificial synaptic devices based on collagen from fish protein with spike-timing-dependent plasticity," Adv. Funct. Mater. **28**, 1800553 (2018).
166. B. Linares-Barranco and T. Serrano-Gotarredona, "Memristance can explain spike-time-dependent-plasticity in neural synapses," Nat. Préc. (2009).
167. X. Yan, Q. Zhao, A. P. Chen, J. Zhao, Z. Zhou, J. Wang, H. Wang, L. Zhang, X. Li, Z. Xiao, K. Wang, C. Qin, G. Wang, Y. Pei, H. Li, D. Ren, J. Chen, and Q. Liu, "Vacancy-induced synaptic behavior in 2D WS_2 nanosheet–based memristor for low-power neuromorphic computing," Small **15**, 1901423 (2019).
168. J.-Y. Chen, X.-G. Tang, Q.-X. Liu, Y.-P. Jiang, W.-M. Zhong, and F. Luo, "An artificial synapse based on $CsPbI_3$ thin film," Micromachines Basel **13**, 284 (2022).
169. L. Zhang, Z. Tang, D. Yao, Z. Fan, S. Hu, Q.-J. Sun, X.-G. Tang, Y.-P. Jiang, X. Guo, M. Huang, G. Zhong, and J. Gao, "Synaptic behaviors in flexible Au/WO_x/Pt/mica memristor for neuromorphic computing system," Mater. Today Phys. **23**, 100650 (2022).
170. J. De Houwer, "The propositional approach to associative learning as an alternative for association formation models," Learn. Behav. **37**, 1–20 (2009).
171. J. M. Pearce and M. E. Bouton, "Theories of associative learning in animals," Annu. Rev. Psychol. **52**, 111–139 (2001).
172. Y. Pei, Z. Zhou, A. P. Chen, J. Chen, and X. Yan, "A carbon-based memristor design for associative learning activities and neuromorphic computing," Nanoscale **12**, 13531–13539 (2020).
173. S. Hu, Y. Liu, Z. Liu, T. Chen, Q. Yu, L. Deng, Y. Yin, and S. Hosaka, "Synaptic long-term potentiation realized in Pavlov's dog model based on a NiO_x-based memristor," J. Appl. Phys. **116**, 214502 (2014).
174. M. Ziegler, R. Soni, T. Patelczyk, M. Ignatov, T. Bartsch, P. Meuffels, and H. Kohlstedt, "An electronic version of Pavlov's dog," Adv. Funct. Mater. **22**, 2744–2749 (2012).
175. J. Zhang, Y. Lu, S. Dai, R. Wang, D. Hao, S. Zhang, L. Xiong, and J. Huang, "Retina-inspired organic heterojunction-based optoelectronic synapses for artificial visual systems," Research Washington DC U.S. 2021, 7131895 (2021).
176. F. Yu, L. Q. Zhu, H. Xiao, W. T. Gao, and Y. B. Guo, "Restickable oxide neuromorphic transistors with spike-timing-dependent plasticity and Pavlovian associative learning activities," Adv. Funct. Mater. **28**, 1804025 (2018).
177. Y. Chen, W. Qiu, X. Wang, W. Liu, J. Wang, G. Dai, Y. Yuan, Y. Gao, and J. Sun, "Solar-blind SnO_2 nanowire photo-synapses for associative learning and coincidence detection," Nano Energy **62**, 393–400 (2019).
178. P. Hökkä, K. Vähäsantanen, and S. Paloniemi, "Emotions in learning at work: a literature review," Vocations Learn. **13**, 1–25 (2020).
179. B. Kort, R. Reilly, and R. W. Picard, "An affective model of interplay between emotions and learning: reengineering educational pedagogy-building a learning companion," in *Proceedings IEEE International Conference on Advanced Learning Technologies* (IEEE, 2001), pp. 43–46.
180. X. Zhou, J. Guo, and R. Bie, "Deep learning based affective model for speech emotion recognition," in *International IEEE Conferences on Ubiquitous Intelligence & Computing, Advanced and Trusted Computing, Scalable Computing and Communications, Cloud and Big Data Computing, Internet of People, and Smart World Congress (UIC/ATC/ScalCom/CBDCom/IoP/SmartWorld)* (IEEE, 2016), pp. 841–846.
181. Y. Wang, W. Huang, Z. Zhang, L. Fan, Q. Huang, J. Wang, Y. Zhang, and M. Zhang, "Ultralow-power flexible transparent carbon nanotube synaptic transistors for emotional memory," Nanoscale **13**, 11360–11369 (2021).
182. J. Zhang, Q. Shi, R. Wang, X. Zhang, L. Li, J. Zhang, L. Tian, L. Xiong, and J. Huang, "Spectrum-dependent photonic synapses based on 2D imine polymers for power-efficient neuromorphic computing," InfoMat **3**, 904–916 (2021).
183. L. Wang and H. Zou, "A new emotion model of associative memory neural network based on memristor," Neurocomputing **410**, 83–92 (2020).
184. L. Huang, L. Wu, Q. Sun, C. Jin, J. Wang, S. Fu, Z. Wu, X. Liu, Z. Hu, J. Zhang, J. Sun, X. Zhu, and Y. Zhu, "All in one: a versatile n-perovskite/p-spiro-meotad p–n heterojunction diode as a photovoltaic cell, photodetector, and memristive photosynapse," J. Phys. Chem. Lett. **12**, 12098–12106 (2021).
185. J. Xue, Z. Zhu, X. Xu, Y. Gu, S. Wang, L. Xu, Y. Zou, J. Song, H. Zeng, and Q. Chen, "Narrowband perovskite photodetector-based image array for potential application in artificial vision," Nano Lett. **18**, 7628–7634 (2018).
186. L. Gu, S. Poddar, Y. Lin, Z. Long, D. Zhang, Q. Zhang, L. Shu, X. Qiu, M. Kam, A. Javey, and Z. Fan, "A biomimetic eye with a hemispherical perovskite nanowire array retina," Nature **581**, 278–282 (2020).
187. J. X. Chen, "The evolution of computing: AlphaGo," Comput. Sci. Eng. **18**, 4–7 (2016).
188. Z. Li, C. Zhu, Y.-L. Gao, Z.-K. Wang, and J. Wang, "AlphaGo policy network: a DCNN accelerator on FPGA," IEEE Access **8**, 203039–203047 (2020).
189. F. Li and Y. Du, "From AlphaGo to power system AI: what engineers can learn from solving the most complex board game," IEEE Power Energy Mag. **16**, 76–84 (2018).
190. G. Wang, R. Wang, W. Kong, and J. Zhang, "Simulation of retinal ganglion cell response using fast independent component analysis," Cogn. Neurodyn. **12**, 615–624 (2018).
191. F. Zhou, Z. Zhou, J. Chen, T. H. Choy, J. Wang, N. Zhang, Z. Lin, S. Yu, J. Kang, H.-S. P. Wong, and Y. Chai, "Optoelectronic resistive random access memory for neuromorphic vision sensors," Nat. Nanotechnol. **14**, 776–782 (2019).